Palaeogeography, Palaeoclimatology, Palaeoecology 512 (2018) 33–45

Contents lists available at ScienceDirect

Palaeogeography, Palaeoclimatology, Palaeoecology

journal homepage: www.elsevier.com/locate/palaeo

Neogene evolution of the north-eastern Tibetan Plateau based on sedimentary, paleoclimatic and tectonic evidence

Yadong Xu[a,b,*], Kexin Zhang[a,b,c,*], Yongfeng Yang[d], Guocan Wang[a,e], Mansheng Luo[b], Junliang Ji[a,b], Bowen Song[c]

[a] School of Earth Sciences, China University of Geosciences, Wuhan 430074, China
[b] State Key Laboratory of Biogeology and Environmental Geology, China University of Geosciences, Wuhan 430074, China
[c] Institute of Geological Survey, China University of Geosciences, Wuhan 430074, China
[d] Region of Shaanxi Bureau of Geology and Mineral Resources and Mineral Research, Xi'an 712000, China
[e] State Key Laboratory of Geological Processes and Mineral Resources, China University of Geosciences, Wuhan 430074, China

ARTICLE INFO

Keywords:
Sedimentary basins
Provenance
Paleocurrent
Middle Miocene climatic optimum
Qilian Shan

ABSTRACT

In this study, the development of the north-eastern Tibetan Plateau is investigated via an integrated study of the sedimentology, magnetostratigraphy, palaeogeography, and cross-section comparisons of the Neogene sedimentary basins of the Tibetan Plateau. From 23 to 17 Ma, this region was characterized by widespread angular unconformities and a sedimentary hiatus, indicating the comprehensive uplift of the plateau. The tectonic event that created the Tibetan Plateau triggered the evolution of sedimentary basins. During the Middle Miocene climatic optimum event, the growing Qilian Shan formed a barrier, leading to cooler and drier conditions on the western side of the mountain. However, humid and warm conditions persisted on the eastern side of the range. After this event, this region was influenced by a global cooling trend and enhanced tectonic activity in the north-eastern Tibetan Plateau. At approximately 10–8 Ma, sedimentary data, which were consistent with low-temperature thermochronological records, indicated the inversion of the surrounding mountains and rapid exhumation of the Laji Shan. Since 5.0–3.6 Ma, these intermontane basins gradually shrank and disappeared due to the overall uplift of the Tibetan Plateau and the accelerated global cooling trend and were associated with unconformities and growth strata that formed during stepwise-north-eastward thrusting tectonism.

1. Introduction

The uplifts of the Tibetan Plateau was accompanied by the formation of Cenozoic intracontinental basins, which can provide valuable insights into the uplift history within the Tibetan Plateau and the associated regional tectonic-climatic coupling (Wang et al., 1999; Fang et al., 2003, 2007a; Pan and Ding, 2004; Dupont-Nivet et al., 2007; Abels et al., 2011; Lease et al., 2012; Miao et al., 2012; Hough et al., 2014; Qi et al., 2016; Song et al., 2018). Many tectonic and climatic events have been documented in the north-eastern Tibetan Plateau (NETP, Fig. 1A), and well-preserved sedimentary sequences have attracted considerable attention over the last decade (Lu and Xiong, 2009; Ge et al., 2012; Wang et al., 2012a, 2012b, 2012c; Zhang et al., 2012; Hough et al., 2014; Chang et al., 2015; Liu et al., 2015; Fang et al., 2016; Miao et al., 2016a, 2016b; Wang et al., 2016a; Zhang et al., 2016; Fu et al., 2017; Ji et al., 2017; Li et al., 2017a, 2017b; Yang et al., 2017; Wang et al., 2018; Zhou et al., 2018). Moreover, many Cenozoic provenance and paleocurrent data have been obtained from research around the NETP, and these data and associated detrital U/Pb zircon analyses (Liu et al., 2013; Nie et al., 2014; Zhang et al., 2014; Bush et al., 2016; Pan et al., 2016; Saylor et al., 2017; Li et al., 2018; Zhou et al., 2018) have been used to track the evolution of the basins.

Many high-resolution chronological studies have been conducted within the NETP (Chang et al., 2001, 2015; Chang, 2004; Sun et al., 2005; Song, 2006; Zhu et al., 2006; Fang et al., 2007a, 2007b, 2016; Meng, 2008; Lu and Xiong, 2009; Wang et al., 2012a, 2012b, 2012c; Zhang et al., 2012; Liu et al., 2015; Hough et al., 2014; Li et al., 2014, 2017a, 2017b; Nie et al., 2014; Song et al., 2014; Zhang et al., 2015a, 2015b; Fang et al., 2016; Miao et al., 2016a, 2016b; Wang et al., 2016a, 2016c, 2017; Fu et al., 2017; Ji et al., 2017; Li et al., 2017a, 2017b; Yang et al., 2017; Song et al., 2018; Wang et al., 2018; Zhou et al., 2018). However, understanding the paleogeographic pattern of the NETP has been hindered due to the lack of high-quality balanced cross-section comparisons. Based on an analysis of regional litho-stratigraphic sequences, the Neogene geological development of the NETP can be divided into four stages (Zhang et al., 2008, 2010a, 2010b,

* Corresponding authors at: State Key Laboratory of Biogeology and Environmental Geology, China University of Geosciences, Wuhan 430074, China.
E-mail addresses: yadong.xu@cug.edu.cn (Y. Xu), kx_zhang@cug.edu.cn (K. Zhang).

https://doi.org/10.1016/j.palaeo.2018.05.012
Received 24 October 2017; Received in revised form 10 May 2018; Accepted 10 May 2018
Available online 17 May 2018
0031-0182/

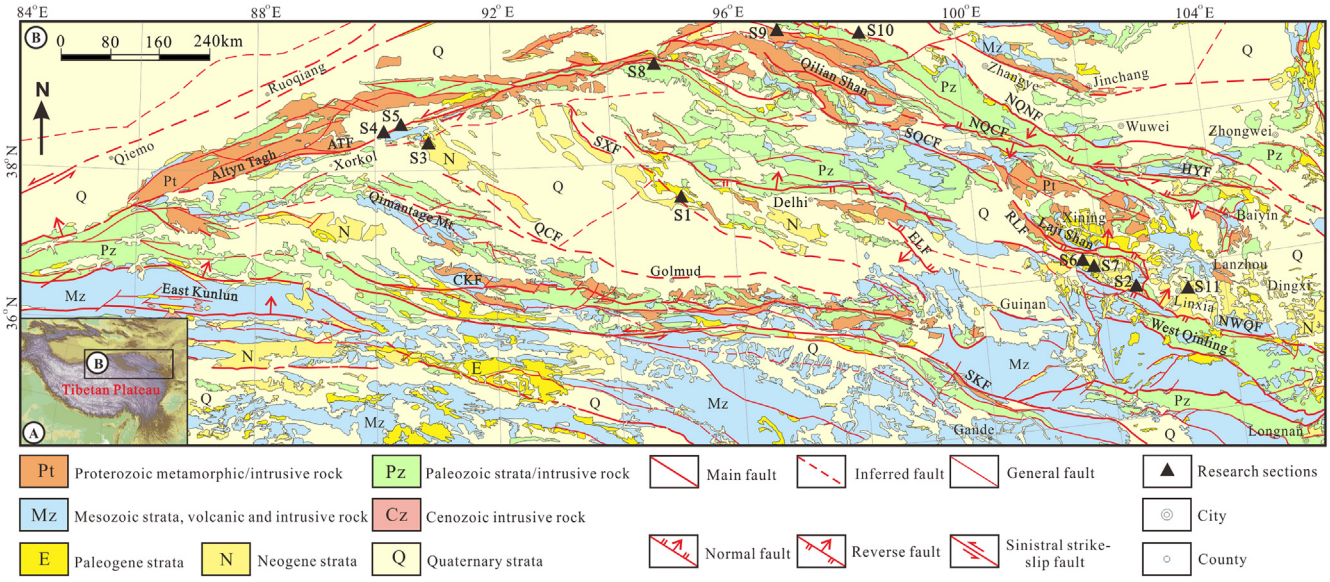

Fig. 1. A DEM map of the Tibetan Plateau and Fig. 1B Geological map of north-eastern Tibetan Plateau (Modified by Pan and Ding, 2004). ATF: Altyn Tagh Fault; CKF: Central East Kunlun Fault; ELF: E'Lashan Fault; HYF: Haiyuan Fault; NQCF: Northern Central Qilian Fault; NQNF: Northern North Qilian Fault; NWQF: Northern West Qinling Fault; QCF: Qaidam Central Fault; RLF: Riyueshan-Lajishan Fault; SKF: Southern East Kunlun Fault; SQCF: Southern Qilian Central Fault; SXF: Shaishiteng Mt.-Xitieshan Fault. S1-S11 show the location and index of the research sections.

2013b; Wang et al., 2011, 2014), in relation to Cenozoic climate changes and the tectonic setting of the surrounding mountains (Ji et al., 2013, 2017; Luo et al., 2013; Xu et al., 2013; Zhang et al., 2013a; Wang et al., 2014; Song et al., 2017). Here we present a comprehensive study of high-quality balanced cross-section comparisons of the remnant basins within the NETP. This paper explores their paleogeographic development of these basins with the Cenozoic tectonic uplift of the surrounding mountains based on statistical analyses of paleocurrent and provenance data.

2. Geological setting

The NETP is an excellent target for paleoenvironmental research in the Tibetan Plateau, which is located at 34°-39°N and 84°-106°E and is bounded by the Altyn Tagh (westward), Qilian Shan-Hexi Corridor (northward), Liupan Shan (eastward), and East Kunlun-West Qinling (southward) (Fig. 1B). These giant mountain ranges and a number of sedimentary basins (including the Qaidam-Delhi, Xorkol, Jiuquan, Subei, Xining, Lanzhou, Guide, Xunhua and Linxia basins) show a tectonic basin-ridge geomorphology.

Several tectonic events have been demonstrated in the NETP, and many main faults around the listed mountain ranges have been research hotspots since the end of the last century. The main faults that have controlled the evolution of the basins are listed in Fig. 1B and include the Altyn Tagh Fault (ATF, Ding et al., 2004; Ritts et al., 2008; Lu and Xiong, 2009; Zhang et al., 2016; Li et al., 2017a, 2017b), Qaidam Central Fault (Cui et al., 1999), Shaishiteng Mountains-Xitieshan Fault (Cui et al., 1999; Wang et al., 2001; Tang et al., 2002), southern Qilian Central Fault (Cui et al., 1995; Chen et al., 1996; Yin et al., 2008a, 2008b; Chen and Li, 2013; Zhang et al., 2017), Riyueshan-Lajishan Fault (Tu et al., 1998; Yuan et al., 2003a, 2003b, 2005, 2006; Liu et al., 2013; Zhang et al., 2015a), and northern West Qinling Fault (Dong et al., 1996; Zhang et al., 2004; Tang et al., 2005; Li et al., 2007).

Furthermore, Cenozoic sedimentary sequences are well preserved in the NETP (Zhang et al., 2010a) and have attracted considerable attention. The ages of the Cenozoic stratigraphic sequence within the NETP have been determined based on high-resolution magnetostratigraphy and palaeontology (mammal and other fossils). Large amounts of Cenozoic provenance and paleocurrent data obtained from the NETP have been used to study the evolution of the basins and their bounding ranges (Chang, 2004; Chang et al., 2015; Sun et al., 2005; Song, 2006; Zhu et al., 2006; Fang et al., 2007b, 2016; Meng, 2008; Lu and Xiong, 2009; Lease et al., 2012; Wang et al., 2012a, 2012b, 2012c; Liu et al., 2013; Jian et al., 2013; Song et al., 2014; Zhang et al., 2014; Zhang et al., 2015a, 2015b). Fang et al. (2005a, 2005b, 2007a, 2016) carried out detailed paleomagnetic research on the Cenozoic strata of the Jiuquan, Linxia, Guide and Xining basins and explored the relationship between the sedimentary evolution and the uplift of the Qilian and Laji Shan. In the Xorkol Basin, detailed Mio-Pliocene lithofacies revealed three regional uplift events (Chang et al., 2001; Chang, 2004). Song et al. (2001, 2003, 2014); Song (2006) statistically analysed data that supported the attitudes of imbricate conglomerate, lenticular glutenite and laminae in cross bedding plots in the Xorkol, Qaidam, Guide and Jiuquan basins to reveal the landform evolution of the NETP. Based on detrital U/Pb zircon analyses, many progress reports have been created to understand the NETP.

3. Methods

The Neogene sedimentary basins in the NETP are filled with many sandstone and conglomerate layers, so this paper aims to conduct detailed basin analyses to detect the growth of the basins in terms of the paleoclimatic and tectonic histories of related mountains via sedimentary facies, balance section reconstruction, paleocurrent and provenance, and other evidence, including tectonic and growth strata data from several representative basins.

To achieve this goal, we 1) measure and/or collect paleocurrent and provenance data from the laminae of cross bedding in sandstone and imbricated conglomerate in 10 sections (Table S1); 2) re-analyse the outcrop-based sedimentary architecture and estimate the structure and litho-facies of the research sequence; 3) apply precious paleomagnetism data alongside new geomagnetic polarity time scale from Ogg (2012) to build a precise chronology for the basin sediments; 4) comparatively analyse sedimentation flux, stable isotope, pollen composition, FT and detrital data to reconstruct the basin's palaeogeography evolution and related mountain denudation history based on the sedimentary and chronological setting.

At each research site, 6-132 paleocurrent measurements were

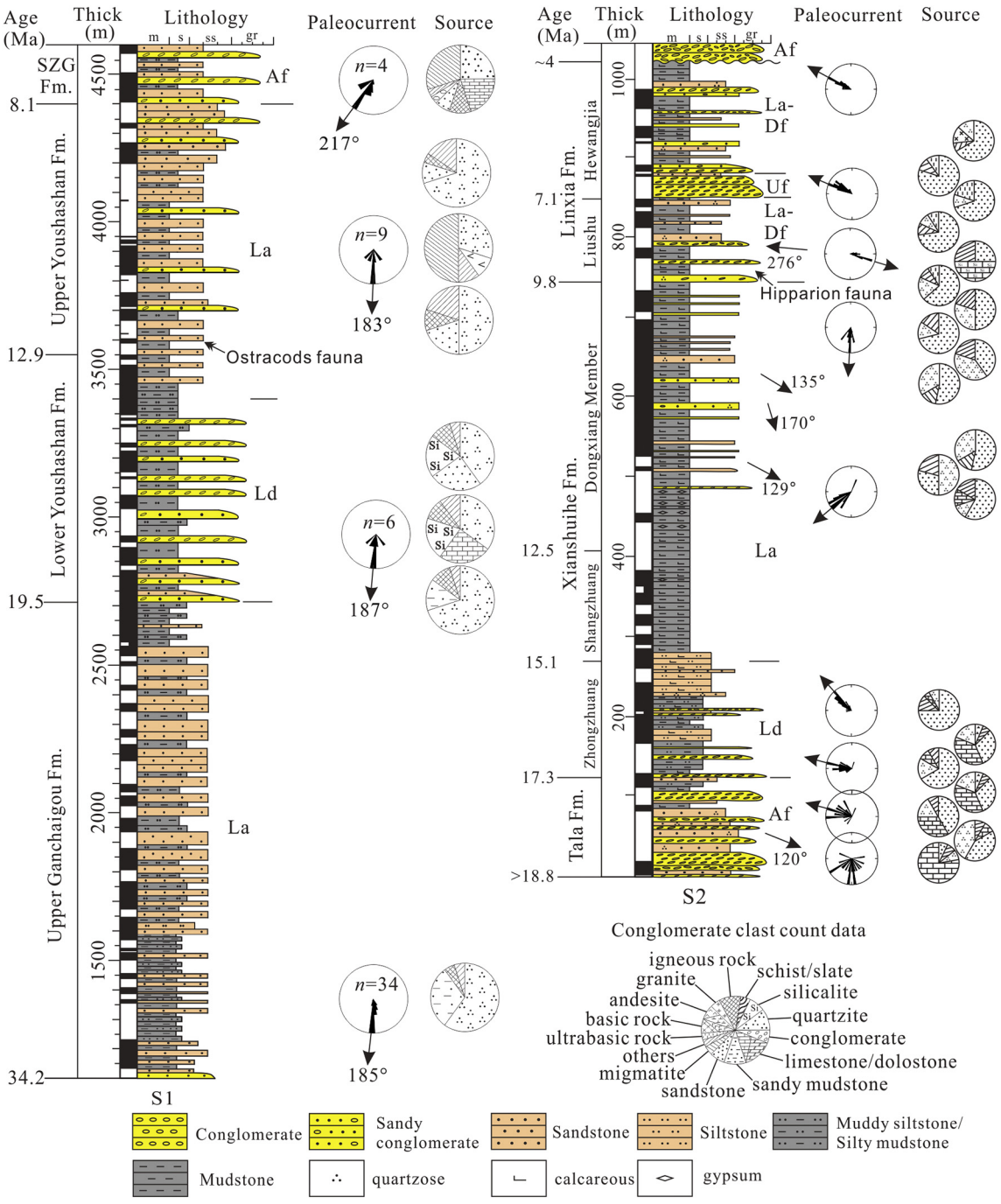

Fig. 2. Neogene stratigraphic column of the Dahonggou Section (S1) and the Xigou Section (S2). The shown magnetostratigraphic data of S1 are from Ji et al. (2017), and the lower and upper magnetostratigraphic data of S2 are from Lease et al. (2012) and Ji et al. (2010), respectively. The ages are bracketed in relation to the geomagnetic polarity time scale (Ogg, 2012). A shift in Ostracods fauna of S1 from *Ilyocypris* to *Cyprideis*, along with the vertebrate fossil *Trilophodon*, constrains the section to the Middle-Late Miocene (Song et al., 2017). The *Hipparion weihoense* of S2 has an age of 9.7–8.7 Ma (Lease et al., 2012). The ages of the intervals were calculated by the linear interpolation method based on the overall age of the sections.

counted, and the measured attitudes of laminae in the plots of cross bedding and flat surfaces of imbricate conglomerate were adjusted by using the Rose 1.0 software, which was developed by Linda DP Thompson and Todd A Thompson in 1993, to derive the horizontal direction of the original deposits and then draw rose diagrams. In addition, detailed statistical analyses of the compositions of abundant conglomerates and sandstones, which were established by using the point-counting method by Suttner and Basu (1985), would show the provenance of the source area, and the results are discussed below. The depositional age of the studied formations was determined from our own studied section S1 (Ji et al., 2017) and S2 (Ji et al., 2010), and previous paleomagnetic data (Chang et al., 2001; Sun et al., 2005; Song, 2006; Ji et al., 2010; Lease et al., 2012; Fang et al., 2016). The ages of the intervals were calculated by the linear interpolation method based on the overall age of the sections.

4. Spatiotemporal characteristics of the paleocurrents and provenance

We measured two sections in the NETP: the Dahonggou section (S1)

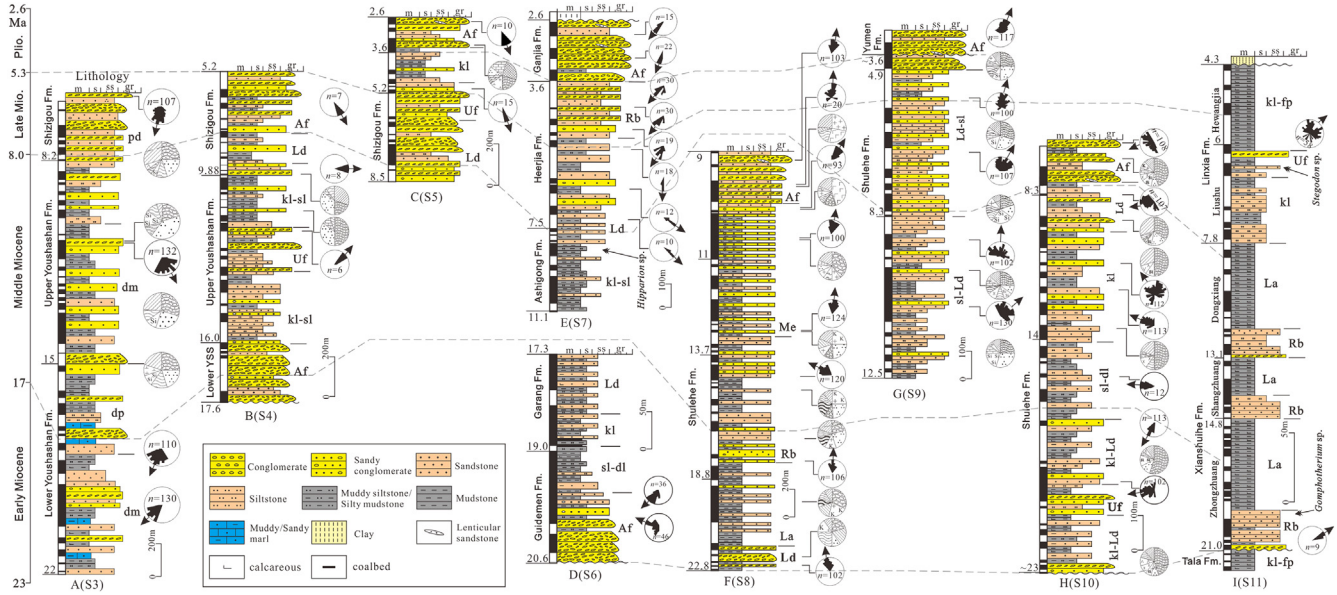

Fig. 3. Mio-Pliocene classic strata comparison and characteristics in the NETP. A. the Xichagou Section S3 in the Qaidam Basin (Song, 2006); B. the Yitunbulake Section S4 in the Xorkol Basin (Chang et al., 2001; Chang, 2004); C. the Xorkol Daban Section S5 in the Xorkol Basin (Chang et al., 2001, Chang, 2004); D. the Ashigong Section S6 in the Guide Basin (Song, 2006); E. the Ganjia Section S7 in the Guide Basin (Song, 2006); F. the Tiejianggou Section S8 in the Subei Basin (Sun et al., 2005; Song, 2006); G. the Laojunmiao Section S9 in the Jiuquan Basin (Song, 2006); H. the Shiyangquan Section S10 in the Jiuquan Basin (Song, 2006); I. the Maogou Section S11 in the Linxia Basin (Fang et al., 2016). Lithofacies: Af, alluvial fan; Me, braided river; Rb, Meandering river; fp, flood plain; Uf, underwater fan; L, Lake; La, saline lake; Ld, lacustrine delta; dp, delta plain; dm, delta front; pd., prodelta; kl, offshore lake; sl, shallow lake; dl, deep lake; Legend for provenance are the same as Fig. 2.

in Dachaidan and the Xigou section (S2) in Xunhua, Qinghai (Fig. 2). Additionally, nine other profiles were selected to carry out a regional comparison (Fig. 3): the Xichagou section (S3) of the Qaidam Basin (Song, 2006), the Yitunbulake section (S4) and the Xorkol Daban section (S5) of the Xorkol Basin (Chang et al., 2001; Chang, 2004), the Ashigong section (S6) and the Ganjia section (S7) of the Guide Basin (Fang et al., 2005a; Song, 2006), the Tiejianggou section (S8) of the Subei Basin (Sun et al., 2005; Song, 2006), the Laojunmiao section (S9) and the Shiyangjuan section (S10) of the Jiuquan Basin (Song, 2006), and the Maogou section (S11) of the Linxia Basin (Yan et al., 2014; Fang et al., 2016). Based on regional comparisons, we can plot the spatio-temporal sedimentary characteristics of these sections, as shown in Figs. 4-7 and described below.

4.1. Dahonggou section

The measured Dahonggou section (S1, 37°29′11″N, 95°12′42″E, Fig. 2) has a thickness of 5400 m and an intact sequence of 584 horizons. This study mainly focuses on the upper unit, which consists of the Upper Ganchaigou Formation (34.2–19.5 Ma), the Youshashan Formation (19.5–8.1 Ma, two members) and the Shizhigou Formation (8.1–2.0 Ma) (Ji et al., 2017). The ages are bracketed in relation to the new geomagnetic polarity time scale (Ogg, 2012). A shift in Ostracods fauna from *Ilyocypris* sp. to *Cyprideis* sp., along with the vertebrate fossil *Trilophodon* sp., constrains the section to the Middle-Late Miocene (Song et al., 2017). Both the Upper Ganchaigou Formation and Upper Youshashan Formation consist of brackish lacustrine facies. The former is dominated by fine-grained lacustrine deposits with a paleocurrent direction of 185°, similar to the direction of 183° for the latter. The grain sizes become finer from the lower to the upper member of the Youshashan Formation, and the paleocurrent directions remain roughly consistent. Moreover, the measured laminae of the cross bedding in the sandstone deposits are mainly oriented SSW and SSE. The gravel mainly comprises quartzite, sandstone, chert and granite, with small amounts of limestone and volcanic products. Therefore, the deposits might be from the South Qilian Shan (Lvliang Shan) on the northern side of the Qaidam Basin. The Shizhigou Formation displays evidence of a series of alluvial coarse-grained deposits. Paleocurrent data show that the flow direction was 217°, which is almost in agreement with paleocurrent data from the Upper Ganchaigou and Youshashan formations (Ji et al., 2017). The compositions of the gravel vary slightly but are still dominated by quartzite, limestone, conglomerate, volcanic products, and other materials. Thus, the source area is the South Qilian Mountains, with no obvious topographic variations.

4.2. Xigou section

The 1047-m Xigou section (S2, 35°48′18 ″N, 102°16′10 ″E, Fig. 2) has a sequence of 213 horizons. The sedimentary units consist of the Tala Formation (> 18.8–17.3 Ma), the Xianshuihe Formation (17.3–9.8 Ma) and the Linxia Formation (9.8–4.0 Ma). The lower and upper magnetostratigraphic data are from Lease et al. (2012) and Ji et al. (2010), respectively. The two magnetostratigraphic sequences were united with the *Hipparion* fauna and were bracketed in relation to the geomagnetic polarity time scale (Ogg, 2012). The *Hipparion weihoense* has an age of 9.7–8.7 Ma (Lease et al., 2012). A series of alluvial fan conglomerates is present in the Tala Formation, which forms the lowest portion of the Xunhua Basin. The paleocurrent directions shift from 120°-188° to 290°-314° (Luo et al., 2010). The compositions of gravel with a NW paleocurrent direction are similar to those of the Permian and Triassic strata in the thrust belt of northern West Qinling (on the southern side of the basin), and those with a SE paleocurrent direction are similar to those of the Proterozoic Hualong Group in Laji Shan (on the northern side of the basin). This observation indicates that both ranges have been high standing since ~19 Ma. The Xianshuihe Formation, with its delta and lacustrine facies, includes three members: the Zhongzhuang Member, Shangzhuang Member and Dongxiang Member. The paleocurrent direction is W-NW in the Zhongzhuang Member and changes to S-SE in the Dongxiang Member (with directions of 129°-190°). The gravel compositions are dominated by sandstone, volcanics, silicolite, quartzite and some metamorphic rocks (Zhang et al., 2010a, 2010b). Provenance data show that the source areas are

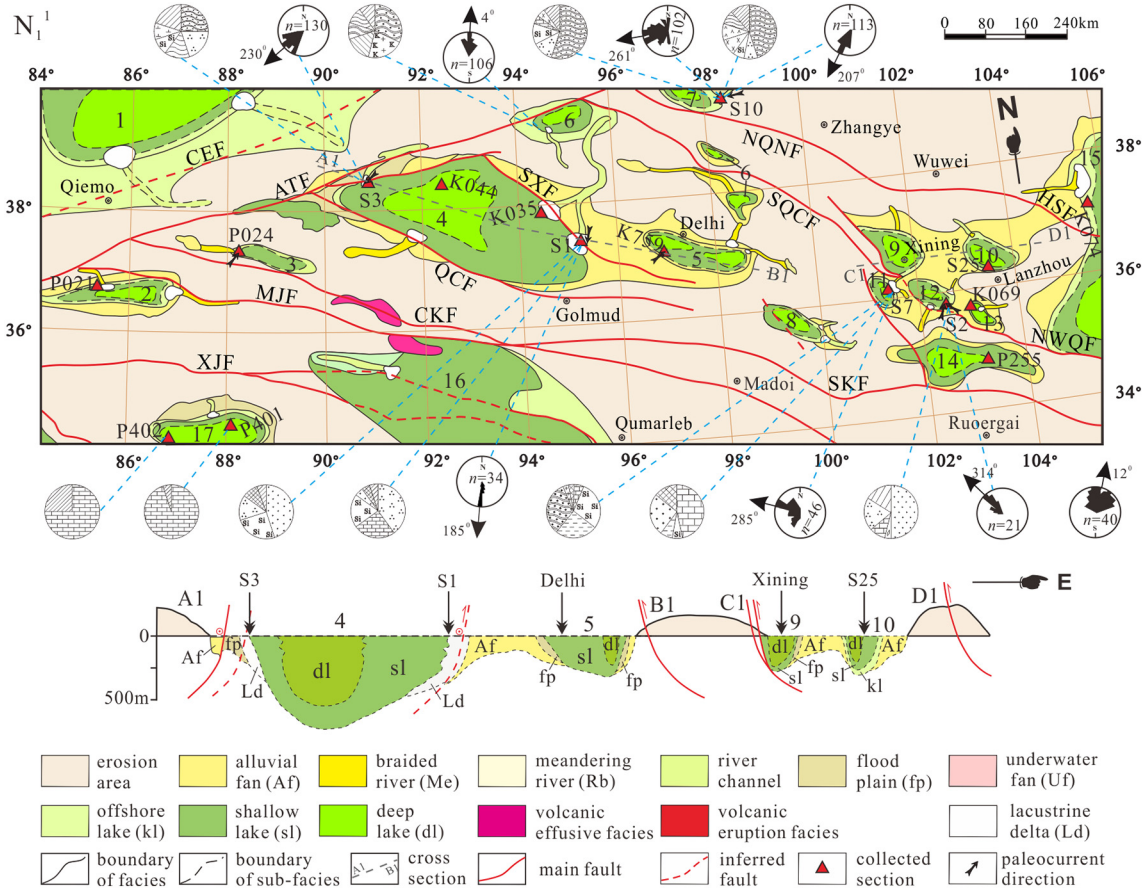

Fig. 4. Early Miocene paleocurrent and lithofacies palaeogeography evolution chart of the research areas. Basin names: 1, Tarim Basin; 2, Aoyiyayilake Basin; 3, Ayakkum Basin; 4, Qaidam Basin; 5, Delhi Basin; 6, Suli Basin; 7, Jiuquan Basin; 8, Xinghai Baisn; 9, Xining Basin; 10, Lanzhou Basin; 11, Guide Basin; 12, Xunhua Basin; 13, Linxia-Dingxi Basin; 14, Zeku-Hezuo Basin; 15, Zhongwei-Tongxin Basin; 16, Wudaoliang- Tuotuohe Basin; 17, Suonahu Basin; CEF: Che'erchen River Fault; MJF: Muzitage- Jingyuhu Fault; XJF: Xijinwulan- Jinshajiang Fault; HSF: Huangcheng- Shuangta Fault. Legend for other faults and provenance are the same as Fig. 1 and Fig. 2, respectively.

the northern West Qinling (southern side) and Laji Shan (northern side). However, in the Zhongzhuang Member, the main source is the northern West Qinling, with stronger source characteristics to the south and weaker characteristics to the north. Subsequently, the topography inverted during the deposition of the Dongxiang Member, and the Laji Shan became the main source area. The overlying Linxia Formation can be divided into two members: the Liushu Member and the Hewangjia Member. These members are dominated by lacustrine and deltaic facies that are intercalated with subaqueous coarse-grained deposits. The paleocurrent direction is mainly WNW (276°, 284°). The gravel compositions are principally sandstone, limestone, granite, quartzite, silicolite, slate, schist and gneiss, with small amounts of mudstone, marble and other ultrabasic rocks, indicating a complex mixture of source areas that include the northern West Qinling on the southern side, the Laji Shan on the northern side, and the Jishi Shan on the eastern side. The top of the section is marked by a series of huge alluvial fan conglomerates in the Jishi Formation since ~4 Ma. The paleocurrent direction is WNW~N, and the gravel clasts consist of sandstone and quartzite (Luo et al., 2010). However, near Hualong County, the direction transitions to 182° and the composition shifts to granite, volcanics, silicolite, mudstone, and other materials (Liu et al., 2007), indicating source areas from the Laji Shan on the northern side.

4.3. Other sections

Based on regional comparisons of our measured sections, four stages of lithofacies, paleocurrents and provenance data can be derived from the other sections within the NETP (Fig. 3; Table S1), as described below.

4.3.1. Early Miocene (23–17 Ma)

During the Early Miocene, shallow lacustrine and deltaic environments, accompanied by alluvial fan conglomerates and sandstones, dominated the NETP. Lacustrine delta deposits exist in the Xichagou area in the western Qaidam Basin (Fig. 3A), and the paleocurrent direction is SW (200°-230°). The conglomerate clasts are mainly meta-sandstone, quartzite, slate and granodiorite (Song, 2006), similar to the compositions of the rocks from the Altyn Tagh (northwest of the basin). In the Huaitoutala section of the Qaidam-Delhi Basin, the paleocurrent direction is NE, indicating that the East Kunlun Mountains were the source area (Meng, 2008). Similarly, paleocurrent data (NW-NNE) for the Shibiliang Formation from Huatiaoshan in the Ayakkum Basin indicate a much greater input from the southern East Kunlun Mountains. A series of huge alluvial fan conglomerates and sandstones are present in the Ashigong (Fig. 3D) and Garang areas in the Guide Basin. The paleocurrent direction is W (285°) (Song et al., 2003; Song, 2006). The clast compositions include sandstone, meta-sandstone, silicolite and limestone around the Guide Gate (Liu et al., 2007). The paleocurrent direction is N around the Tiejianggou area in the Subei Basin (Fig. 3F), which is dominated by lacustrine deposits. The Shiyangjuan area of the southern Jiuquan Basin (Fig. 3H) is also dominated by fine-grained lacustrine deposits that are interbedded with subaqueous fan facies. The paleocurrent direction is W (261°-274°). The provenance is mainly meta-sandstone, quartzite, silicolite, diabase and andesite, with some

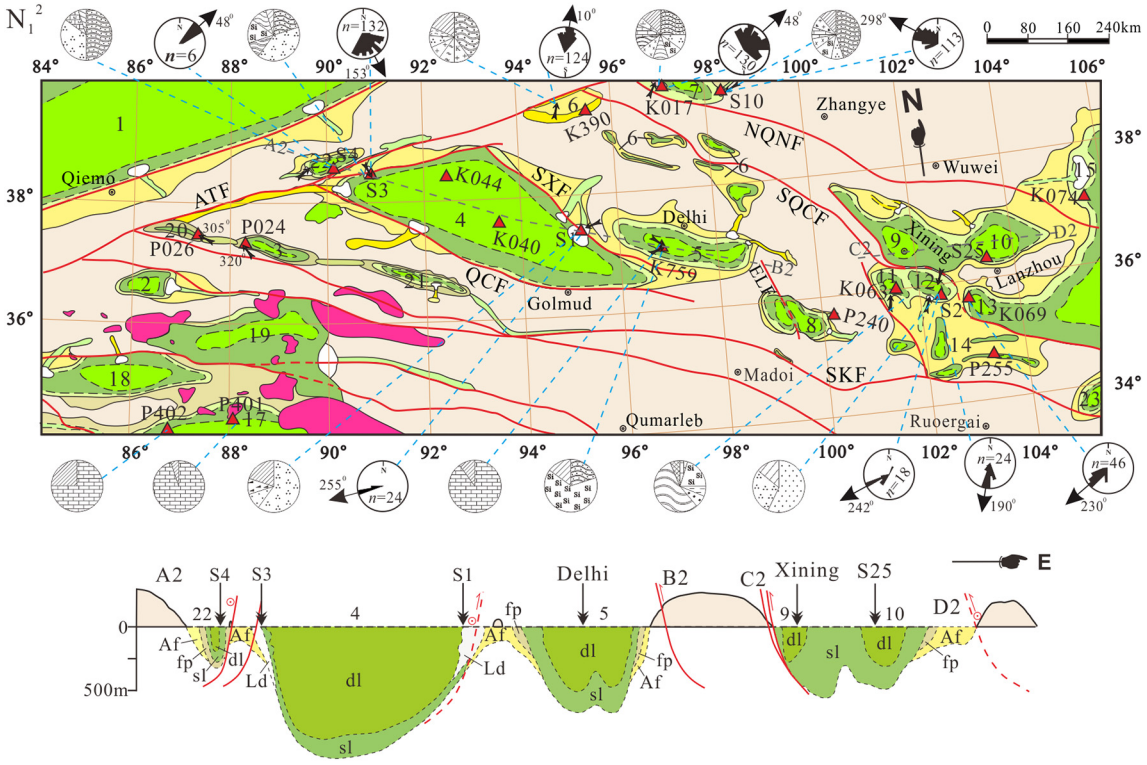

Fig. 5. Middle Miocene paleocurrent and lithofacies palaeogeography evolution chart of the research area. Basin names: 18, Margai Caka Basin; 19, Hoh Xil Basin; Other Legend in the chart are the same as Fig. 2 and Fig. 4.

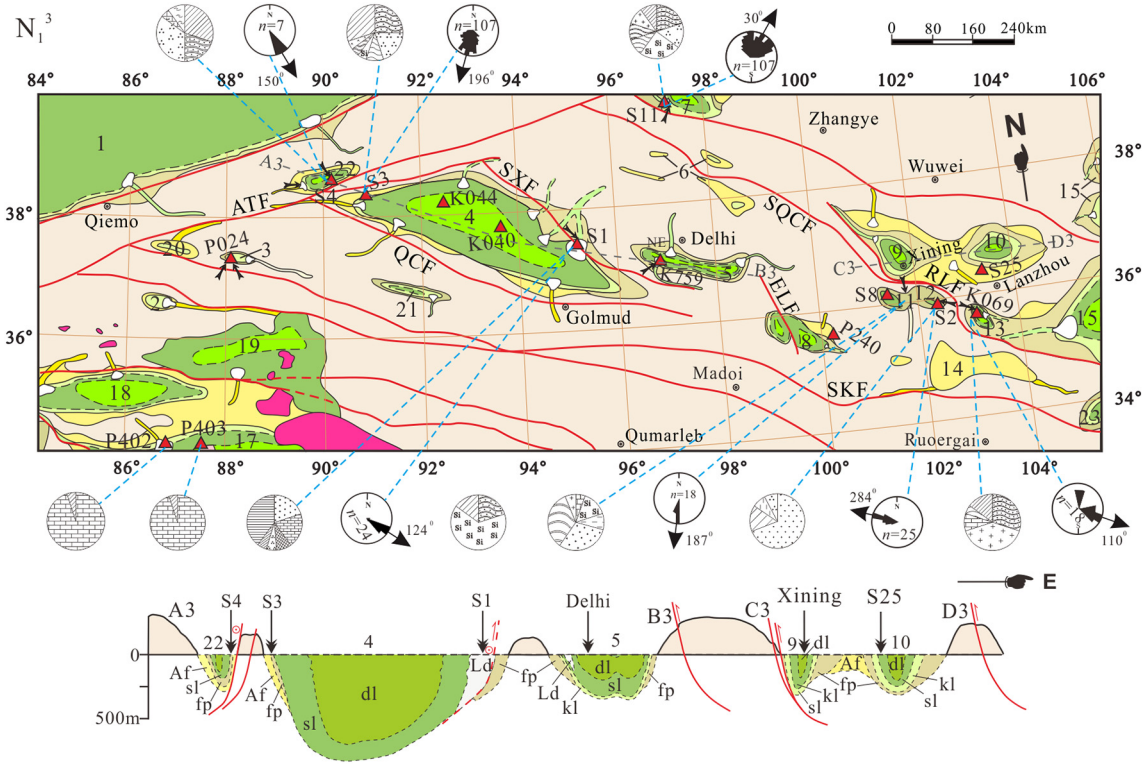

Fig. 6. Late Miocene lithofacies provenance and palaeogeography evolution chart of the research area. Basin names: 20, Kezisay Basin; 21, Buluntai Basin; 22, Xorkol Basin; 23, Longnan Basin; Other Legend in the chart are the same as Fig. 2 and Figs. 4-5.

limestone and schist and rare migmatite and moyite (Song et al., 2001; Song, 2006). Therefore, the source area is the North Qilian Mountains on the eastern side of the basin (Fig. 4). In the Linxia Basin, the recorded paleocurrent direction in the Zhongzhuang Member around Maogou, Dongxiang County, is 12°-59° (Fig. 3I, Fang et al., 1997, 2007a, 2016). Therefore, the main source area was the West Qinling Mountains on the southern side of the basin, with the initial uplift of the Laji Shan occurring on the western side of the basin (Fig. 4).

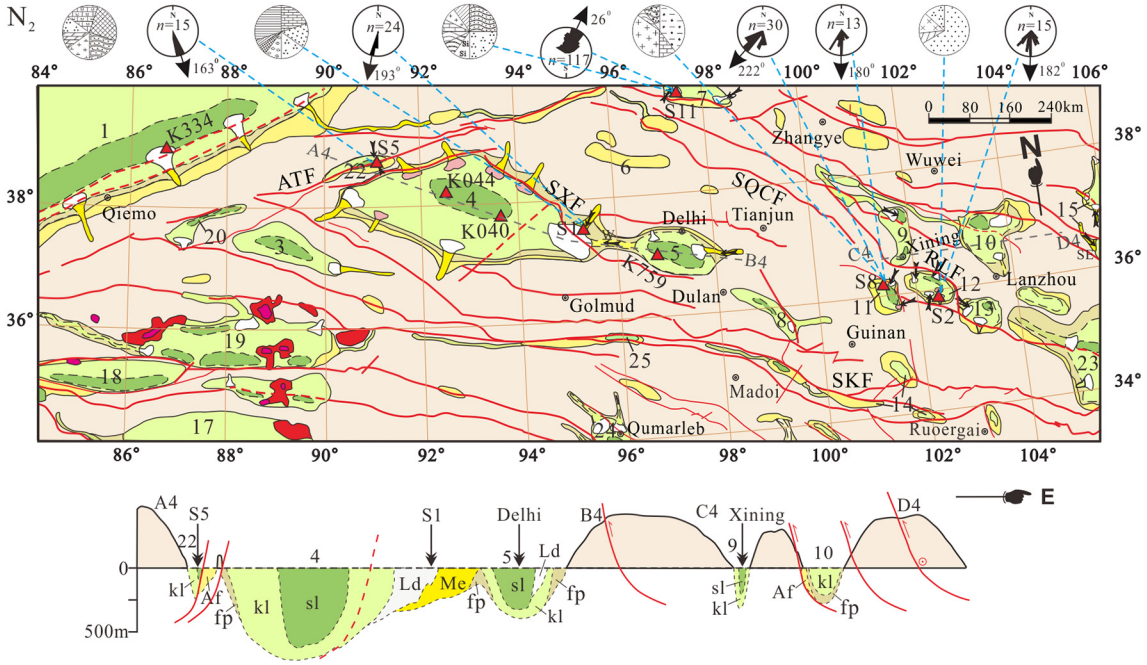

Fig. 7. Pliocene provenance and lithofacies palaeogeography evolution chart of the research area. Basin names: 24, Qumarleb Basin; 25, East Hot Spring Basin. Other Legend in the chart are the same as Fig. 2 and Figs. 4-6.

4.3.2. Middle Miocene (17–8 Ma)

During the Middle Miocene, the lacustrine environment of the NETP changed to deep or semi-deep, several small lakes formed a unified basin, and the Xorkol Basin began to accumulate deposits. In the Xorkol Basin, the first facies were alluvial fans, shifting to offshore-shallow lacustrine sediments that were interbedded with subaqueous fan facies (Fig. 3B). Around the southern side of the basin, the paleocurrent direction is NE (48°), and the clasts are mostly tuffaceous sandstone, meta-sandstone and quartzite (Chang et al., 2001; Ge et al., 2002, 2006). The uplifted areas were the Altyn Tagh on the western side of the basin and the Qimantage Mountains on the southern side of the basin. The Qaidam-Delhi Basin was a united basin, and the western area around Ganchaigou-Xichagou, Mangya, was dominated by lacustrine delta facies with paleocurrents that were oriented to the SE (132°) (Fig. 3A). The clasts are predominantly quartzite, meta-sandstone, silicolite, slate, schist, and other similar materials (Song, 2006). However, the paleocurrent direction on the eastern side of the basin, 10 km south of Huaitoutala, is mainly NE-SE, and the conglomerate clasts consist of limestone in the lower section and silicolite and meta-sandstone in the upper section (Meng, 2008), indicating that the source areas were the Altyn Tagh and South Qilian Shan (Aimunike Mountains) (Fig. 5). Similarly, a unified basin also formed around the Guide-Linxia Basin. In the Xunhua area, the paleocurrent direction was S-SW during the early stages (Luo et al., 2010) and changed to SE and SW (129°-190°, 242°) during the later stages (Fig. 3E), with clasts that consist of sandstone, volcanics, silicolite, quartzite and some metamorphic rocks (Zhang et al., 2010a, 2010b). In the Linxia area, the paleocurrent direction is NNE around the Guonigou and Heilinding (Fang et al., 2016), which may be comparable to the data from Maogou (Fig. 3I). Therefore, this basin received sediment from the West Qinling to the south. The Tiejianggou area features river to alluvial fan facies, with NW or N paleocurrent direction and a new basalt component (Fig. 3F). In contrast, the Jiuquan Basin features a semi-deep to shallow lake that is sandwiched between delta fan facies. This sequence has paleocurrent directions of NE (48°) to N (355°) in the Laojunmiao area (Fig. 3G), and gravel compositions of meta-sandstone, silicolite, quartzite, schist, limestone and diabase (Song et al., 2001; Song, 2006). The paleocurrent directions changes from NW (298°, 336°) to SW (264°) in the Shiyangjuan area (Fig. 3H), and the clasts are predominantly meta-sandstone, silicolite and quartzite. Therefore, the main source area was the Qilian Shan on the south-western and south-eastern side of the basin (Fig. 5).

4.3.3. Late Miocene (8–5.3 Ma)

During this period, the major sedimentary basins shrank and formed coarse clastic deposits in the NETP. In the Xorkol Basin, alluvial fan facies are present at Yitunbulake (Fig. 3B) and offshore-shallow lacustrine facies are present at Xorkol Daban (Fig. 3C), and the paleocurrent direction is SE (163°). Multiple sediment sources were involved based on the appearance of granite, granodiorite and mafic volcanics (Chang et al., 2001; Ge et al., 2002, 2006). These data show that the source area was the Altyn Tagh on the western side of the basin (Fig. 6). The Qaidam Basin shows stable shallow lacustrine facies across the basin. However, a lake delta existed in the Xichagou area (Fig. 3A), with an S-oriented paleocurrent direction (196°). The conglomerate clasts are mainly meta-sandstone, quartzite, slate and granodiorite (Song, 2006), indicating that the northern side of the basin (South Qilian Shan) had been uplifted. In the Delhi area, the paleocurrent direction of the Huaitoutala is NE, which shows that the East Kunlun Mountains to the southwest of the basin were the source area (Meng, 2008). A series of huge lake delta facies exists in the Ganjia and Garang areas in the Guide Basin (Fig. 3E). The paleocurrent directions are SE-S (123°-187°) (Song et al., 2003; Song, 2006). The clasts transition to sandstone, meta-sandstone, silicolite and limestone around the Guide Gate (Liu et al., 2007). Therefore, these data indicate the uplift of the Laji Shan on the northern side of the basin (Fig. 6). Offshore-shallow lacustrine to delta facies are found near Laojunmiao in the Jiuquan Basin (Fig. 3G), which have NNE (20°-30°) paleocurrent directions. The clasts mainly include meta-sandstone, quartzite, silicolite, limestone, schist, and other materials (Song, 2006). Therefore, the source area was close to the southern Qilian Mountains. The paleocurrent is oriented SW (248°) in the Shiyangjuan area (Fig. 3H), and the clasts are predominantly meta-sandstone, with upwardly increasing proportions of diabase, andesite porphyry, meta-conglomerate and schist. The main source area was still the Qilian Shan (Fig. 6). In the Linxia area, the paleocurrent is oriented SE at the Maogou area (Fig. 3I), and the gravels mainly consist of

sandstone, quartzite, granite, silicolite and schist (Fang et al., 2016).

4.3.4. Pliocene (5.3–2.6 Ma)

Following the last stage, these major sedimentary basins began to shrink and accumulate coarse clastic deposits. Shallow lacustrine to alluvial fan facies are found at Xorkol Daban (Fig. 3C). The paleocurrent direction shifts to the SE (158°–163°), and the conglomerate clasts include meta-sandstone, siliceous limestone, dolomite, granodiorite, gabbro and mafic volcanic rocks (Chang, 2004), indicating the further uplift of the north-western Jinyan Shan as the material source area (Chang et al., 2001; Chang, 2004; Chen et al., 2006; Song, 2006). Fan delta to alluvial fan facies and the highest sedimentation rate are found in the Qigequan area in the Qaidam Basin. The paleocurrent direction changed from northward during the previous period to southward during the Pliocene (Song, 2006). However, the conglomerate clast data are quite complicated and indicate source areas on the northern side of the Altyn Tagh and the South Qilian Shan. Due to the intense thrusting that occurred in the surrounding mountains, braided river to alluvial fan facies with SW paleocurrent directions (197°–220°) developed in the Ganjia area in the Guide Basin (Fig. 3E). However, these facies transition to delta and shallow-lake facies in the southern area of the basin and are accompanied by finer grain sizes and thinner layers of conglomerate. The paleocurrent shifts to the S (180°) on the northern side of the basin and to the N on the southern side of the basin around Wajiacun (Song et al., 2003, Song, 2006). A series of alluvial fan conglomerates likely exist in the Xunhua-Hualong Basin. On the northern side of the basin, the paleocurrent direction shifts to the S (182°), and the clast compositions include granite, volcanic rocks, chert and mudstone (Liu et al., 2007). On the southern side, the paleocurrent direction shifts to the WNW or N, and the clasts are sandstone and quartzite (Luo et al., 2010). Therefore, the source areas were the West Qinling on the southern side, the Laji Shan on the northern side, and the Jishi Shan on the eastern side (Fig. 7). A series of alluvial fans with a northward paleocurrent direction are observed in the southern Jiuquan Basin. The clast composition differs from that of the previous stage, with increases in the proportions of sandstone and meta-sandstone and decreases in the proportions of quartzite and granite (Fig. 3G), and the paleocurrent direction shifts to the NE (26°) (Song et al., 2001, Song, 2006). Therefore, the North Qilian Mountains had clearly been uplifted. However, the facies are still offshore lake-flood plain facies around the Maogou area (Fig. 3I).

5. Discussion

5.1. Framework of the sedimentary basins before 17 Ma

Many data recorded the intense uplift of the Tibetan Plateau during 23–17 Ma (Zhang et al., 2014). Simultaneously, the subsidence of the sedimentary basins in the NETP was significant (Lease et al., 2012; Liu et al., 2015). Tectonic factors could have triggered the evolution of the sedimentary basins, which are characterized by widespread angular unconformities and sedimentary hiatuses (Zhang et al., 2008, 2013b; Xiao et al., 2012; Liu et al., 2015). These observations, in conjunction with low-temperature thermochronological records (Zhong and Ding, 1996; Wang et al., 2011; Song et al., 2014), indicate the overall uplift of the NETP since the Neogene. Along the ATF, intensive exhumation and cooling events between 22 and 17 Ma occurred in the Qiemo-Mangai (Chen et al., 2006) and Qiman areas (Bai et al., 2008). Jolivet et al. (2001) suggested a tectonic heating record of approximately 22–18 Ma in the Qilian Shan. Correspondingly, the paleocurrent directions were consistently oriented to the south in the Upper Ganchaigou Formation and Youshashan Formation, and the gravel composition was the same as that from the South Qilian Shan and Altyn Tagh. However, the source area around the Huaitoutala and Huatiaoshan was the East Kunlun Mountains. The northern West Qinling thrust fault moved northward to the Laji Shan during 21–16 Ma (Liu et al., 2013; Lease et al., 2012), and accelerated exhumation was also recorded at 18 Ma (Clark et al., 2010). Thermochronological age-elevation transects data also indicated that the accelerated exhumation of the eastern Laji Shan occurred at approximately 22 Ma (Lease et al., 2011; Xiao et al., 2012). The subsidence of the newly formed Xunhua-Guide Basin resulted in the development of alluvial fans (such as the Tala Formation and Guidemen Formation). The paleocurrent directions and the compositions of gravel indicated that both the West Qinling and the Laji Shan were the source areas (Fig.2), which were the same as those of the Linxia Basin. Moreover, stable isotopic data from the Xunhua Basin were generally consistent with the values from the Linxia Basin for 20.3–16.6 Ma (Hough et al., 2011), indicating a large unified basin around the Xunhua-Linxia area (i.e., the Jishi Shan did not exist yet). This area was dominated by lacustrine deposits in the Jiuquan Basin, and the source area was the North Qilian Shan on the eastern side. At 18 Ma, potassic and adakitic volcanism occurred in the western Qiangtang and Songpan-Ganze areas (Xia et al., 2011), indicating the northward progression of magmatic activity that was related to the Indian lithosphere.

A cooling and drying trend has existed in the NETP region since the Neogene (Guo et al., 2002, 2008; Lease et al., 2012; Song et al., 2017; Zhang et al., 2014) based on the aeolian dust and mineral content index data. A similar arid climate occurred during 23–18 Ma in the western Qaidam Basin (Wang et al., 1999) and the Tarim Basin (Tang et al., 2011) based on pollen records. In contrast, the global $\delta^{18}O$ values decreased during 20–17 Ma (Zachos et al., 2001; Fig. 8A), indicating a warming trend. Moreover, the Paratethys Sea did not completely retreat in western China until the Late Oligocene (Zhang et al., 2007; Zhang et al., 2013b) or even the Early Miocene (Rögl, 1998; Zhang et al., 2008). However, other data indicated that the closure of the Paratethys Sea had a minor influence on climate change in north-western China (Wang et al., 1999). Hence, the uplift of the Tibetan Plateau likely triggered aridification in the Asian inland (Miao et al., 2012; Zhang et al., 2015a, 2015b) and influenced the evolution of the Neogene sedimentary basins.

5.2. Basin expansion during 17–8 Ma

The Middle Miocene climatic optimum (MMCO) event occurred during 17–14.7 Ma (Tian et al., 2014; Holbourn et al., 2015), which had a great influence on basin development in the NETP. The mean annual temperature of the Northern Hemisphere (de Boer et al., 2010) and chemical index of alteration in the South China Sea (Wan et al., 2007; Fig. 8G) increased during this event. Within the NETP, the sedimentary sag area expanded, as evidenced by the formation of the offshore-shallow Xorkol Basin, and several small lakes formed a unified basin that was dominated by lacustrine delta facies (Fig. 5).

However, the NETP could be divided into two components across the Qilian Shan (Fig. 8E) based on differences in the geological and climatic records. First, an accelerating decrease in the total organic carbon concentrations and an increase in concentrations of the soluble anions SO_4^{2-} and Cl^- during 17–11.1 Ma on the western side of the Qilian Shan (Song et al., 2014) accompanied by the gradual drying and salinization of the western Qaidam Basin. Miao et al. (2012) concluded that pollen data and other proxies in Central Asia and the surrounding region indicated that the climate on the western side of the Qilian Shan experienced drying and cooling trends starting at 17 Ma (based on sections C1–C7 in their paper). Therefore, although the paleo-lakes expanded and deepened, the records from the western side of the Qilian Shan suggested cooling and drying trends during the MMCO event.

On the eastern side of the Qilian Shan, gypsum veins disappeared at 17.5 Ma in the northern portion of the Xunhua Basin (Lease et al., 2012; Fig. 2) and at 16 Ma on the southern side of the basin (appearing again after 10 Ma) (Hough et al., 2011). The delta and lacustrine facies indicated a large unified basin in the Xunhua-Linxia area, precluding the existence of the Jishi Shan (Zhang et al., 2010a, 2010b; Lease et al., 2012). In the Xining Basin, the magnetic susceptibility (χ) data

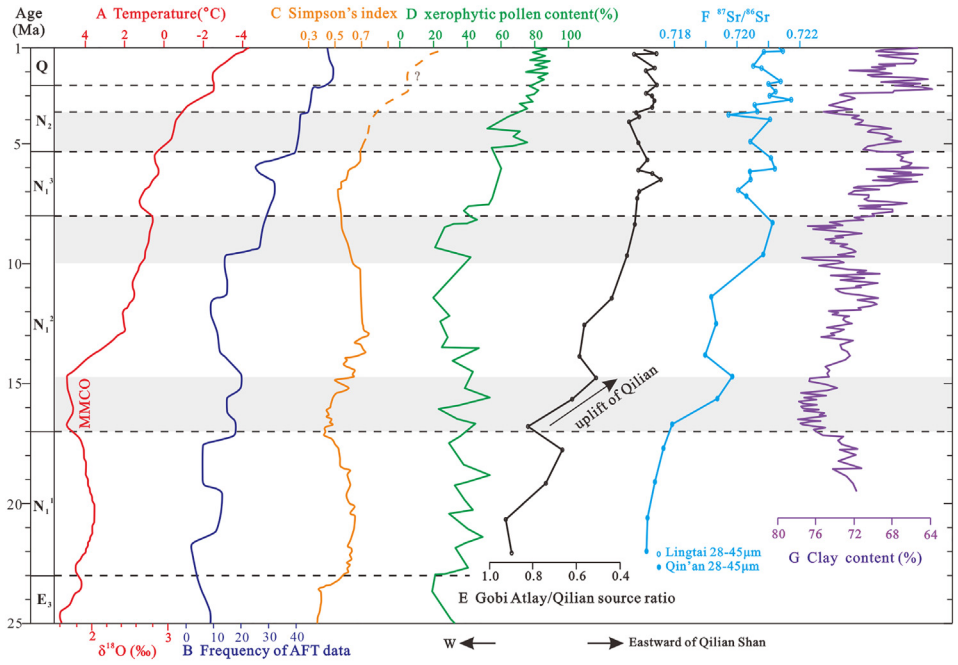

Fig. 8. Variations of paleoclimatic and tectonic data discussed in this paper. A. global marine oxygen isotope $\delta^{18}O$ values and paleotemperature curve (Zachos et al., 2001); B. frequency of AFT data around the Tibetan Plateau (Wang et al., 2011; Zhang et al., 2013b); C. simpson's diversity index of the palynological records of central Asia (Tang et al., 2011); D. xerophytic pollen (including *Pteris*, Polypodiaceae, *Ephedra*, Chenopodiaceae, *Nitraria* and *Artemisia*) percentage of total pollen count of the Qaidam Basin (Wang et al., 1999); E. Nd–Sr isotopic ratio of source contribution from Qilian Mt. and Gobi Altay and F. silicate Sr isotopic data of the aeolian dust in Qin'an and Lingtai, respectively (Chen and Li, 2013); G. relative weight percents of clay minerals in terrigenous components at ODP Site 1146 in the northern South China Sea (Wan et al., 2007), to see detailed discussion in the paper.

fluctuated considerably with the high sedimentation rate during 17–16 Ma (Xiao et al., 2012). In contrast, the χ values in the Qin'an and Zhuanglang areas were noticeably high during 17–14 Ma (Guo et al., 2002; Qiang et al., 2011). Furthermore, the thermophilic pollen taxa of the Linxia Basin and the Zhongwei Basin showed increasing trends (Fang et al., 2003; Jiang and Ding, 2008), which were consistent with increases in the temperature and precipitation of the East Asia (Miao et al., 2012). The high relative humidity index reflected greater precipitation and greater fluvial input from the surrounding uplifted areas during the MMCO event.

Third, apatite FT data recorded the uplift of the central Qilian Shan during 17–14 Ma (Wang et al., 2011, Fig. 8B; Zhang et al., 2013b; Zheng et al., 2017), and extensive exhumation in the Qilian Shan occurred at 18–8 Ma (Qi et al., 2016; He et al., 2017; Wang et al., 2017; Zhuang et al., 2018). The rapid uplift of the Qilian Shan was also observed from detrital provenance analysis at ~16 Ma (Wang et al., 2016b; Wang et al., 2017) and Sr isotopic compositions (Chen and Li, 2013; Fig. 8E). The progressive north-eastward growth of the Qilian Shan since 17 Ma was recorded by thermochronological data (Li et al., 2015; Qi et al., 2016; Zheng et al., 2017), and then upward deformation transitioned stepwise to the Laji Shan and northward-trending Jishi Shan during 17–13 Ma (Lease et al., 2011).

The westward aridification of the Qilian Shan could be interpreted in two ways: (1) the growing Qilian Shan created a rain shadow that contrasted with the intensification of the Asian summer monsoon, and (2) the uplift of the Tibetan Plateau caused increased aridity in the Asian interior during the MMCO.

After the MMCO event, an unconformity existed between the Youshashan Formation and the Shizigou Formation at approximately 11–10 Ma, and the facies changed to fan deltas with sulphidic conditions in the western Qaidam Basin (Song et al., 2014). Moreover, the uplift of the Qimantage Mountains was recorded by the paleocurrent direction and clasts from the Xorkol Basin and western Qaidam Basin, which divided the Qaidam Basin and Ayakekum Basin during ~15–8 Ma (Zhou et al., 2018). A clear sedimentary deformation formed at approximately 15 Ma (Wang et al., 2012a, 2012b, 2012c; Wu et al., 2012) in the western Qaidam Basin, and the source areas were the Altyn Tagh and south Qilian Shan on the eastern side of the united Qaidam-Delhi Basin. Simultaneously, the sedimentary strata rotated clockwise by ~50° during ~16.2–11.1 Ma of at the Yitunbulake area (Li et al., 2017a, 2017b) and by 25° during 17–11 Ma in the Guide Basin (Yan et al., 2006). In the Jiuxi Basin, deep- to shallow-lake facies formed in the Laojunmiao area during 13–8.26 Ma (Song et al., 2001, Fig. 3), which were accompanied by low sedimentation rates. The calcite cements and carbonates of the deposits show positive oxygen isotopic shifts during the mid-Miocene in the Linxia Basin (Garzione et al., 2004), suggesting that the moisture source moved into the Asian interior (An et al., 2001; Zhang et al., 2013). Additionally, the topography inverted during 15–13.1 Ma around the Linxia Basin as the main source area shifted from the West Qinling to the Laji Shan. The Xining Basin changed from an extensional pull-apart basin to a compressive intermontane basin during a major inversion stage at 17–8 Ma (Zhang et al., 2014), which was accompanied by the rapid exhumation of the Laji Shan (Zhang et al., 2015a, 2015b).

5.3. Shrinking period of depressed basins after 8 Ma

These sedimentary basins in the NETP rapidly shifted from lacustrine to fluvial-alluvial basins starting at 8.0 Ma, and alluvial fan facies were found at Xorkol Daban, Ganjia and Laojunmiao (Fig. 3). In the Xining Basin, the lithofacies transitioned from floodplain to braided-river facies at ~8.6 Ma and then to a thick alluvial fan at ~6.3 Ma, with southern paleocurrent directions around Mojiazhuang (Yang et al., 2017). Since 7.8 Ma, this area was dominated by lacustrine and deltaic facies that were intercalated with coarse-grained deposits of the Linxia Basin. The gravel compositions and paleocurrent data showed a complex mixture of source areas, indicating the uplift of the West Qinling (southern side), the Laji Shan (northern side) and the Jishi Shan (eastern side). At this time, a clear decrease in the aeolian sand content occurred in the Linxia Basin (Wang et al., 1999; Fig. 8D). The basin rotated clockwise by approximately 10° (Fang et al., 2003) and experienced a distinct change in magnetic susceptibility from haematite dominated to magnetite dominated at 8.5 Ma in the Heilinding area (Yan et al., 2014) and at 6.0 Ma in the Maogou region (Yan et al., 2006). At the same time, the Asian continental interior experienced a short dry interval (Derbyshire et al., 1998), and alluvial fans widely developed in the northern Qaidam Basin (Zhuang et al., 2011). At approximately 8 Ma, the Cenozoic strata along the Altyn Tagh and Liupan Shan experienced fault-related deformation and became steeply tilted (Wang et al., 2010), forming growth strata over an angular unconformity (Fang

et al., 2005a, 2005b; Zhang et al., 2013; Li et al., 2014). This deformation was accompanied by the first appearance of conglomerate that was intercalated with gravelly sandstone in the western Qaidam Basin. Thus, the lake area began to shrink at approximately 8.0–6.5 Ma (Fang et al., 2007b). At 8.0 Ma, the tree cover rapidly decreased in the NETP and was replaced by an expansion of grass and shrubs (Li et al., 2014). The first occurrence of C_4 biomass was concurrently recorded at the Qaidam Basin (Zhang et al., 2012) and in other locations globally (Quade et al., 1989; Cerling et al., 1997). The expansion of C_4 plants around the NETP may have been influenced by the Asian interior's aridity at 8 Ma. Strong activity along the ATF was recorded at 10–7 Ma (Wan et al., 2001; Chen et al., 2002; Wang et al., 2002) and 5.0 Ma (Chen et al., 2002; Wang et al., 2011). A rapid exhumation-related cooling event in the Qilian Shan occurred at 9–5 Ma (Jolivet et al., 2001). In the Laji Shan, Liupan Shan and East Kunlun Mountains, a rapid exhumation (uplift) event occurred at 8.0–5.4 Ma (Zheng et al., 2003; Lease et al., 2007; Zheng et al., 2010; Li et al., 2014). Correspondingly, the Laji Shan and Qilian Shan were the main provenance regions for the Xining Basin's sediment during the Miocene, as determined through detrital zircon U−Pb data (Zhang et al., 2014).

A comprehensive review by Li et al. (2014) noted that synchronous variations in grain size, conglomerate content, sedimentation rate and climatic proxies were also recorded at 8.0 Ma, 3.6 Ma and 2.6 Ma around the NETP (Fang et al., 2005a; Zhang et al., 2010a, 2010b; Li et al., 2014), which were associated with changes in sedimentary facies from shallow lakes, lake deltas and braided rivers to high-relief alluvial fans. Intermontane basins occurred throughout the NETP since 3.6 Ma, as documented by unconformities in the Ganjia, Laojunmiao, and Maogou areas, which were associated with the formation of growth strata formed during northward thrusting around the Qilian Shan (Zheng et al., 2017). The shrinking of the Guide and Linxia basins was marked by the accumulation of huge alluvial fan conglomerates since 3.8 Ma (Pares et al., 2003). We demonstrated that the major forcing factors of the stepwise drying and shrinking of these sedimentary basins at 8.0 Ma, 5.3 Ma, 3.6 Ma and 2.6 Ma were regional tectonism, but we cannot preclude the obvious influence of global cooling since 8 Ma (Fig. 8A). This examination is a chicken-and-egg situation and is a longstanding challenge that requires further clues.

6. Conclusions

The geological evolution of the NETP was recorded in its associated basins. An integrated study of the sedimentary, paleocurrent, provenance, and paleogeographic data from the Neogene sedimentary basins provided a detailed record of the growth of the NETP. From 23 to 17 Ma, the NETP was characterized by widespread angular unconformities and sedimentary hiatuses that were accompanied by arid climatic conditions, indicating the widespread uplift of the NETP, which triggered the evolution of the sedimentary basins. During the MMCO event, on the western side of the Qilian Shan, a cooling and drying period occurred in the Qaidam and Tarim areas on the western side of the Qilian Shan and in Central Asia. However, large unified basins formed under the humid and warm conditions on the eastern side of the mountains because the growing Qilian Mountains formed a barrier that blocked moisture from the East Asia, causing aridification on the western side. Subsequently, the region was also controlled by a global cooling trend. At approximately 10–8 Ma, the grain size and sedimentation rates of these basins abruptly increased, which is consistent with the low-temperature thermochronology records and indicates the rapid uplift of the surrounding mountains. Furthermore, the provenance data of the Guide, Xunhua and Linxia basins indicated the uplift of the Jishi Shan. After 3.6 Ma, these sedimentary basins shrank and gradually disappeared because of the widespread uplift of the Tibetan Plateau and the accelerated global cooling trend.

Supplementary data to this article can be found online at https://doi.org/10.1016/j.palaeo.2018.05.012.

Acknowledgments

We thank An Wang and Junsheng Nie for their valuable discussions of data interpretation and assistance with writing the manuscript. We are also grateful to Editor Thomas Algeo and Zhongshi Zhang, reviewer Yunfa Miao and another anonymous reviewer for their suggestions to improve the manuscript. This research was funded by the National Special Project on the Tibetan Plateau of the Geological Survey of China (Nos. 121201004000150013, DD20160345, 1212011121261) and the National Natural Science Foundation of China (Nos. 41302279, 41602037).

References

Abels, H.A., Dupont-Nivet, G., Xiao, G.Q., Bosboom, R., Krijgsman, W., 2011. Step-wise change of Asian interior climate preceding the Eocene-Oligocene transition (EOT). Palaeogeogr. Palaeoclimatol. Palaeoecol. 299, 399–412.

An, Z.S., Kutzbach, J.E., Prell, W.L., Porter, S.C., 2001. Evolution of Asian monsoons and phased uplift of the Himalaya-Tibetan plateau since Late Miocene times. Nature 411, 62–66.

Bai, Y.S., Ren, E.F., Fan, G.L., Xu, C.Q., 2008. Apatite fission track evidence for the Miocene rapid uplift of the Qimantag Mountains on the northwestern margin of the Qinghai-Tibet plateau. Geol. Bull. China 27, 1044–1048 (in Chinese with English abstract).

de Boer, B., de Wal, R.S.W., Bintanja, R., Lourens, L.J., Tuenter, E., 2010. Cenozoic global ice-volume and temperature simulations with 1-D ice-sheet models forced by benthic $\delta^{18}O$ records. Ann. Glaciol. 51, 23–33.

Bush, M.A., Saylor, J.E., Horton, B.K., Nie, J.S., 2016. Growth of the Qaidam Basin during Cenozoic exhumation in the northern Tibetan plateau: inferences from depositional patterns and multiproxy detrital provenance signatures. Lithosphere 8, 58–82.

Cerling, T.E., Harris, J.M., MacFadden, B.J., Leakey, M.G., Quade, J., Elsenmann, V., Ehlerlnger, J.R., 1997. Global vegetation change through the Miocene/Pliocene boundary. Nature 389, 153–158.

Chang, H., 2004. Research on Late Cenozoic Magneticstratigraphy in the Xorkol Basin along the Atlyn Tagh and Uplift of North Tibetan Plateau. Doctoral Dissertation of Institute of Earth Environment. Chinese Academy of Sciences, Beijing, pp. 45–65 (in Chinese with English abstract).

Chang, H., Fang, X.M., An, Z.S., Song, C.H., Qiang, X.K., 2001. Miocene-Pliocene strata features in the Suerkal Basin and the palaeo-environment significance. Mar. Geol. Quat. Geol. 21, 107–111 (in Chinese with English abstract).

Chang, H., Li, L.Y., Qiang, X.K., Garzione, C.N., Pullen, A., An, Z.S., 2015. Magnetostratigraphy of Cenozoic deposits in the western Qaidam Basin and its implication for the surface uplift of the northeastern margin of the Tibetan plateau. Earth Planet. Sci. Lett. 430, 271–283.

Chen, Z., Li, G.J., 2013. Evolving sources of eolian detritus on the Chinese loess plateau since early Miocene: tectonic and climatic controls. Earth Planet. Sci. Lett. 371–372, 220–225.

Chen, B.W., Yao, P.Y., Guo, X.P., Liu, X., Dong, X.B., 1996. Tectonics and Evolution of Terraces in the North Part of the Qinghai-Xizang (Tibet) Plateau. Geological Publishing House, Beijing, pp. 69–79 (in Chinese).

Chen, Z.L., Wan, J.L., Wang, X.F., Chen, X.H., Pan, J.H., 2002. Rapid strike-slip of the AltynTagh fault at 8 Ma and its geological implications. Acta Geosci. Sin. 23, 295–300 (in Chinese with English abstract).

Chen, Z.L., Gong, H.L., Li, L., Wang, X.F., Chen, B.L., Chen, X.H., 2006. Cenozoic uplifting and exhumation process of the Altyn Tagh Mountains. Earth Sci. Front. 13, 91–102 (in Chinese with English abstract).

Clark, M.K., Farley, K.A., Zheng, D.W., Wang, Z.C., Duvall, A.R., 2010. Early Cenozoic faulting on the northern Tibetan plateau margin from apatite (U–Th)/He ages. Earth Planet. Sci. Lett. 296, 78–88.

Cui, Z.Z., Li, Q.S., Wu, C.D., Yin, Z.X., Liu, H.B., 1995. The crustal and deep structures in Golmud-Ejin Qi GCT. Acta Geophys. Sin. 38, 15–28 (in Chinese with English abstract).

Cui, J.W., Tang, Z.M., Deng, J.F., Yue, Y.J., Meng, L.S., Yu, Q.F., 1999. Altun fault system. Geological Publishing House, Beijing, pp. 1–315 (in Chinese).

Derbyshire, E., Meng, X.M., Kemp, R.A., 1998. Proenance, transport and characteristics of modern Aeolian dust in western Gansu Province, China, and interpretation of the Quaternary loess record. J. Arid Environ. 39, 497–516.

Ding, G.Y., Chen, J., Tian, Q.J., Shen, X.H., Xing, C.Q., Wei, K.B., 2004. Active faults and magnitudes of left-lateral displacement along the northern margin of the Tibetan plateau. Tectonophysics 380, 243–260.

Dong, Z.P., Lei, F., Shen, X.R., Ma, L.H., 1996. The deep structure features of the fault zone along northern edge of West Qinling and its relation with seismic activity. Inland Earthq. 10, 224–234 (in Chinese with English abstract).

Dupont-Nivet, G., Krijgsman, W., Langereis, C.G., Abels, H.A., Dai, S., Fang, X.M., 2007. Tibetan plateau aridification linked to global cooling at the eocene-oligocene transition. Nature 445, 635–638.

Fang, X.M., Li, J.J., Zhu, J.J., Chen, H.L., Cao, J.X., 1997. Absolute dating and division of Cenozoic strata in Linxia basin, Gansu Province. Chin. Sci. Bull. 42, 1457–1471 (in Chinese with English abstract).

Fang, X.M., Garzione, C.N., Van der Voo, R., Li, J.J., Fan, M.J., 2003. Flexural subsidence by 29 Ma on the NE edge of Tibet from the magnetostratigraphy of Linxia Basin,

China. Earth Planet. Sci. Lett. 210, 545–560.
Fang, X.M., Yan, M.D., Voo, R., Rea, D.K., Song, C.H., Pares, J.M., Gao, J.P., Nie, J.S., Dai, S., 2005a. Late Cenozoic deformation and uplift of the NE Tibetan plateau: evidence from high- resolution magnetostratigraphy of the Guide Basin, Qinghai Province, China. Geol. Soc. Am. Bull. 117, 1208–1225.
Fang, X.M., Zhao, Z.J., Li, J.J., Yan, M.D., Pan, B.T., Song, C.H., Dai, S., 2005b. Magnetostratigraphy of the late Cenozoic Laojunmiao anticline in the northern Qilian Mountains and its implications for the northern Tibetan plateau uplift. Sci. China Ser. D Earth Sci. 48, 1040–1051.
Fang, X.M., Song, C.H., Dai, S., Zhu, Y.T., Gao, J.P., Zhang, W.L., 2007a. Cenozoic deformation and uplift of the NE Qinghai-Tibet plateau: evidence from high-resolution magnetostratigraphy and basin evolution. Earth Sci. Front. 14, 230–242 (in Chinese with English abstract).
Fang, X.M., Zhang, W.L., Meng, Q.Q., Gao, J.P., Wang, X.M., King, J., Song, C.H., Dai, S., Miao, Y.F., 2007b. High-resolution magnetostratigraphy of the Neogene Huaitoutala section in the eastern Qaidam Basin on the NE Tibetan plateau, Qinghai Province, China and its implication on tectonic uplift of the NE Tibetan plateau. Earth Planet. Sci. Lett. 258, 293–306.
Fang, X.M., Wang, J.Y., Zhang, W.L., Zan, J.B., Song, C.H., Yan, M.D., Appel, E., Zhang, T., Wu, F.L., Yang, Y.B., Lu, Y., 2016. Tectonosedimentary evolution model of an intracontinental flexural (foreland) basin for paleoclimatic research. Glob. Planet. Chang. 145, 78–97.
Fu, C.F., Qiang, X.K., Xu, X.W., Xi, J.J., Zuo, J., An, Z.S., 2017. Late Miocene magnetostratigraphy of Jianzha Basin in the northeastern margin of the Tibetan plateau and changes in the East Asian summer monsoon. Geol. J. 1–11. http://dx.doi.org/10.1002/gj.3047.
Garzione, C.N., Dettman, D.L., Horton, B.K., 2004. Carbonate oxygen isotope paleoaltimetry: evaluating the effect of diagenesis on paleoelevation estimates for the Tibetan plateau. Palaeogeogr. Palaeoclimatol. Palaeoecol. 212, 119–140.
Ge, X.H., Liu, Y.J., Ren, S.M., 2002. Uplift dynamics of Qinghai-Tibet plateau and Altyn fault. Geol. China 29, 346–350 (in Chinese with English abstract).
Ge, X.H., Ren, S.M., Ma, L.X., Wu, G.D., Liu, Y.J., Yuan, S.H., 2006. Multi-stage uplifts of the Qinghai-Tibet plateau and their environmental effects. Earth Sci. Front. 13, 118–130 (in Chinese with English abstract).
Ge, J.Y., Guo, Z.T., Zhan, T., Yao, Z.Q., Deng, C.L., Oldfield, F., 2012. Magnetostratigraphy of the Xihe loess-soil sequence and implication for late Neogene deformation of the West Qinling Mountains. Geophys. J. Int. 189, 1399–1408.
Guo, Z.T., Ruddiman, W.F., Hao, Q.Z., Wu, H.B., Qiao, Y.S., Zhu, R.X., Peng, S.Z., Wei, J.J., Yuan, B.Y., Liu, T.S., 2002. Onset of Asian desertification by 22 Myr ago inferred from loess deposits in China. Nature 416, 159–163.
Guo, Z.T., Sun, B., Zhang, Z.S., Peng, S.Z., Xiao, G.Q., Ge, J.Y., Hao, Q.Z., Qiao, Y.S., Liang, M.Y., Liu, J.F., Yin, Q.Z., Wei, J.J., 2008. A major reorganization of Asian climate by the early Miocene. Clim. Past 4, 153–174.
He, P.J., Song, C.H., Wang, Y.D., Chen, L.H., Chang, P.F., Wang, Q.Q., Ren, B., 2017. Cenozoic exhumation in the Qilian Shan, northeastern Tibetan plateau: evidence from detrital fission track thermochronology in the Jiuquan Basin. J. Geophys. Res. Solid Earth 122, 6910–6927.
Holbourn, A., Kuhnt, W., Kochhann, K.G.D., Andersen, N., Sebastian Meier, K.J., 2015. Global perturbation of the carbon cycle at the onset of the Miocene climatic optimum. Geology 43, 123–126.
Hough, B.G., Garzione, C.N., Wang, Z.C., Lease, R.O., Burbank, D.W., Yuan, D.Y., 2011. Stable isotope evidence for topographic growth and basin segmentation: implications for the evolution of the NE Tibetan plateau. Geol. Soc. Am. Bull. 123, 168–185.
Hough, B.G., Garzione, C.N., Wang, Z.C., Lease, R.O., 2014. Timing and spatial patterns of basin segmentation and climate change in northeastern Tibet. Geol. Soc. Am. Spec. Pap. 507, 129–153.
Ji, J.L., Zhang, K.X., Qiang, T., Kou, X.H., Chen, F.N., Xu, Y.D., Lu, J.F., Lin, Q.X., 2010. Magnetostratigraphy of the Neogene strata in Xunhua Basin, Qinghai Province. Earth Sci. 35, 803–810 (in Chinese with English abstract).
Ji, J.L., Jiang, S.S., Zhang, K.X., Chen, F.N., Wang, G.C., Yang, Y.F., Luo, M.S., 2013. Pliocene tectonics and lithofacies paleogeography of the Tibetan plateau. Geol. Bull. China 32, 19–30 (in Chinese with English abstract).
Ji, J.L., Zhang, K.X., Clift, P.D., Zhuang, G.S., Song, B.W., Ke, X., Xu, Y.D., 2017. High-resolution magnetostratigraphic study of the Paleogene-Neogene strata in the Northern Qaidam Basin: implications for the growth of the northeastern Tibetan plateau. Gondwana Res. 46, 141–155.
Jian, X., Guan, P., Zhang, D.W., Zhang, W., Feng, F., Liu, R.J., Lin, S.D., 2013. Provenance of Tertiary sandstone in the northern Qaidam basin, northeastern Tibetan plateau: integration of framework petrography, heavy mineral analysis and mineral chemistry. Sediment. Geol. 290, 109–125.
Jiang, H.C., Ding, Z.L., 2008. A 20 Ma pollen record of East-Asian summer monsoon evolution from Guyuan, Ningxia, China. Palaeogeogr. Palaeoclimatol. Palaeoecol. 265, 30–38.
Jolivet, M., Brunel, M., Seward, D., Xu, Z., Yang, J., Roger, F., Tapponnier, P., Malavieille, J., Arnaud, N., Wu, C., 2001. Mesozoic and Cenozoic tectonics of the northern edge of the Tibetan plateau: fission track constraints. Tectonophysics 343, 111–134.
Lease, R.O., Burbank, D.W., Gehrels, G.E., Wand, Z.C., Yuan, D.Y., 2007. Signatures of mountain building: detrital zircon U/Pb ages from northeastern Tibet. Geology 35, 239–242.
Lease, R.O., Burbank, D.W., Clark, M.K., Farley, K.A., Zheng, D., Zhang, H., 2011. Middle Miocene reorganization of deformation along the northeastern Tibetan plateau. Geology 39, 359–362.
Lease, R.O., Burbank, D.W., Hough, B., Wang, Z.C., Yuan, D.Y., 2012. Pulsed Miocene range growth in northeastern Tibet: insights from Xunhua Basin magnetostratigraphy and provenance. Geol. Soc. Am. Bull. 124, 657–677.
Li, C.Y., Zhang, P.Z., Zhang, J.X., Yuan, D.Y., Wang, Z.C., 2007. Late-Quaternary activity and slip rate of the Western Qinling fault zone at Huangxianggou. Quat. Res. 27, 54–63 (in Chinese with English abstract).
Li, J.J., Fang, X.M., Song, C.H., Pan, B.T., Ma, Y.Z., Yan, M.D., 2014. Late Miocene-Quaternary rapid stepwise uplift of the NE Tibetan Plateau and its effects on climatic and environmental changes. Quat. Res. 81, 400–423.
Li, Y.L., Wang, C.S., Dai, J.G., Xu, G.Q., Hou, Y.L., Li, X.H., 2015. Propagation of the deformation and growth of the Tibetan-Himalayan orogeny: a review. Earth Sci. Rev. 143, 36–61.
Li, J.J., Ma, Z.H., Li, X.M., Peng, T.J., Guo, B.H., Zhang, J., Song, C.H., Liu, J., Hui, Z.C., Yu, H., Ye, X.Y., Liu, S.P., Wang, X.X., 2017a. Late Miocene-Pliocene geomorphological evolution of the Xiaoshuizi peneplain in the Maxian Mountains and its tectonic significance for the northeastern Tibetan plateau. Geomorphology 295, 393–405.
Li, B.S., Yan, M.D., Zhang, W.L., Fang, X.M., Meng, Q.Q., Zan, J.B., Chen, Y., Zhang, D.W., Yang, Y.P., Guan, C., 2017b. New paleomagnetic constraints on middle Miocene strike-slip faulting along the middle Altyn Tagh Fault. J. Geophys. Res. Solid Earth 122, 4106–4122.
Li, L.L., Wu, C.D., Yu, X.J., 2018. Cenozoic evolution of the Altyn Tagh and East Kunlun fault zones inferred from detrital garnet, tourmaline and rutile in southwestern Qaidam Basin (Northern Tibetan plateau). Basin Res. 30, 35–58.
Liu, S.F., Zhang, G.W., Heller, P.L., 2007. The development and the indicating function from Xunhua- Guide Cenozoic basin. Sci. China Ser. D Earth Sci. 37, 235–248.
Liu, S.F., Zhang, G.W., Pan, F., Zhang, H.P., Wang, P., Wang, K., Wang, Y., 2013. Timing of Xunhua and Guide basin development and growth of the northeastern Tibetan plateau, China. Basin Res. 25, 74–96.
Liu, S.P., Li, J.J., Stockli, D.F., Song, C.H., Nie, J.S., Peng, T.J., Wang, X.X., He, K., Hui, Z.C., Zhang, J., 2015. Late Tertiary reorganizations of deformation in northeastern Tibet constrained by stratigraphy and provenance data from eastern Longzhong Basin. J. Geophys. Res. Solid Earth 120, 5804–5821.
Lu, H.J., Xiong, S.F., 2009. Magnetostratigraphy of the Dahonggou section, northern Qaidam Basin and its bearing on Cenozoic tectonic evolution of the Qilian Shan and Altyn Tagh fault. Earth Planet. Sci. Lett. 288, 539–550.
Luo, M.S., Zhang, K.X., Lin, Q.X., Zhang, J.Y., Chen, F.N., Xu, Y.D., Chen, R.M., 2010. Cenozoic sedimentary paleogeography evolution of Xunhua-Hualong area, northwestern Qinghai-Tibet plateau. Geol. Sci. Technol. Info. 29, 23–31 (in Chinese with English abstract).
Luo, M.S., Zhang, K.X., Xu, Y.D., Wang, G.C., Chen, R.M., Chen, F.N., Song, B.W., Zhang, J.Y., Yang, Y.F., 2013. Miocene tectonic lithofacies paleogeography of the Tibetan plateau. Geol. Bull. China 32, 31–43 (in Chinese with English abstract).
Meng, Q.Q., 2008. High Resolution Magnetostratigraphy in the North of Qaidam Basin and the Sedimentary Response to Tectonic since Late Cenozoic. Doctoral dissertation of Lanzhou University, Gansu. pp. 1–142 (in Chinese with English abstract).
Miao, Y.F., Herrmann, M., Wu, F.L., Yan, X.L., Yang, S.L., 2012. What controlled mid-late Miocene long-term aridification in Central Asia? Global cooling or Tibetan plateau uplift: a review. Earth Sci. Rev. 112, 155–172.
Miao, Y.F., Fang, X.M., Liu, Y.S., Yan, X.L., Li, S.Y., Xia, W.M., 2016a. Late Cenozoic pollen concentration in the western Qaidam Basin, northern Tibetan plateau, and its significance for paleoclimate and tectonics. Rev. Palaeobot. Palynol. 231, 14–22.
Miao, Y.F., Fang, X.M., Song, C.H., Yan, X.L., Zhang, P., Meng, Q.Q., Li, F., Wu, F.L., Yang, S.L., Kang, S.Y., Wang, Y.P., 2016b. Late Cenozoic fire enhancement response to aridification in mid-latitude Asia: evidence from microcharcoal records. Quat. Sci. Rev. 139, 53–66.
Nie, J.S., Peng, W.B., Moller, A., Song, Y.G., Stockli, D.F., Stevens, T., Horton, B.K., Liu, S.P., Bird, A., Oalmann, J., Gong, H.J., Fang, X.M., 2014. Provenance of the upper Miocene-Pliocene red clay deposits of the Chinese loess plateau. Earth Planet. Sci. Lett. 407, 35–47.
Ogg, J.G., 2012. Geomagnetic polarity time scale. In: Gradstein, F.M., Ogg, J.G., Schmitz, M., Ogg, G. (Eds.), The Geological Time Scale 2012. Vol. 2012. Elsevier, Amsterdam, pp. 5–113.
Pan, G.T., Ding, J., 2004. Geological Map of the Qinghai-Tibetan Plateau and its Adjacent Area (1: 150, 0000). Chengdu Cartographic Publishing House, Chengdu, pp. 1–60.
Pan, F., Li, J.X., Xu, Y., Yue, L.P., Wingate, M.T.D., Li, Y.G., Guo, L., Xi, R.G., Guo, L., 2016. Provenance of Neogene eolian red clay in the Altun region of western China-insights from U-Pb detrital zircon age data. Palaeogeogr. Palaeoclimatol. Palaeoecol. 459, 488–494.
Pares, J.M., Voo, R., Downs, W.R., Yan, M.D., Fang, X.M., 2003. Northeastward growth and uplift of the Tibetan plateau: magnetostratigraphic insights from the Guide Basin. J. Geophys. Res. Solid Earth 108 (B1). http://dx.doi.org/10.1029/2001JB001349.
Qi, B.S., Hu, D.G., Yang, X.X., Zhang, Y.L., Tan, C.X., Zhang, P., Feng, C.J., 2016. Apatite fission track evidence for the Cretaceous-Cenozoic cooling history of the Qilian Shan (NW China) and for stepwise northeastward growth of the northeastern Tibetan plateau since early Eocene. J. Asian Earth Sci. 124, 28–41.
Qiang, X.K., An, Z.S., Song, Y.G., Chang, H., Sun, Y.B., Liu, W.G., Ao, H., Dong, J.B., Fu, C.F., Wu, F., 2011. New aeolian red clay sequence on the western Chinese loess plateau linked to onset of Asian desertification about 25 Ma ago. Sci. China Ser. D Earth Sci. 54, 136–144.
Quade, J., Cerling, T.E., Bowman, J.R., 1989. Development of Asian monsoon revealed by marked ecological shift during the latest Miocene in northern Pakistan. Nature 342, 163–166.
Ritts, B.D., Yue, Y.J., Graham, S.A., 2008. From sea level to high elevation in 15 million years:uplift history of the northern Tibetan plateau margin in the Altun Shan. Am. J. Sci. 308, 657–678.
Rögl, V.F., 1998. Palaeogeographic considerations for Mediterranean and Paratethys seaways (Oligocene to Miocene). Ann. Naturhist. Mus. Wien 99A, 279–310.
Saylor, J.E., Jordan, J.C., Sundell, K.E., Wang, X.M., Wang, S.Q., Deng, T., 2017. Topographic growth of the Jishi Shan and its impact on basin and hydrology evolution, NE Tibetan plateau. Basin Res. 1–20. http://dx.doi.org/10.1111/bre.12264.

Song, C.H., 2006. Tectonic Uplift and Cenozoic Sedimentary Evolution in the Northern Margin of the Tibetan Plateau. Doctoral dissertation of Lanzhou University, Gansu. pp. 1–325 (in Chinese with English abstract).
Song, C.H., Fang, X.M., Li, J.J., Gao, J.P., Zhao, Z.J., Fan, M.J., 2001. Tectonic uplift and sedimentary evolution of the Jiuxi Basin in the northern margin of the Tibetan plateau since 13 Ma BP. Sci. China Ser. D Earth Sci. 44, 192–202.
Song, C.H., Fang, X.M., Li, J.J., Gao, J.P., Sun, D., Fan, M.J., Yan, M.D., 2003. Pliocene sedimentary environment of the Guide basin on the northeast margin of the Qinghai-Tibetan plateau and its significance. Quat. Sci. Rev. 23, 92–102 (in Chinese with English abstract).
Song, C.H., Hu, S.H., Han, W.X., Zhang, T., Fang, X.M., Gao, J.P., Wu, F.L., 2014. Middle Miocene to earliest Pliocene sedimentological and geochemical records of climate change in the western Qaidam Basin on the NE Tibetan plateau. Palaeogeogr. Palaeoclimatol. Palaeoecol. 395, 67–76.
Song, B.W., Ji, J.L., Wang, C.W., Xu, Y.D., Zhang, K.X., 2017. Intensified aridity in the Qaidam Basin during the Middle Miocene: constraints from ostracod, stable isotope and weathering records. Can. J. Earth Sci. 54, 242–256.
Song, Y.G., Fang, X.M., Chen, X.L., Torii, M., Ishikawa, N., Zhang, M.S., Yang, S.L., Chang, H., 2018. Rock magnetic record of late Neogene red clay sediments from the Chinese loess plateau and its implications for east Asian monsoon evolution. Palaeogeogr. Palaeoclimatol. Palaeoecol. http://dx.doi.org/10.1016/j.palaeo.2017a.09.025. (in press).
Sun, J.M., Zhu, R.X., An, Z.S., 2005. Tectonic uplift in the northern Tibetan plateau since 13.7 Ma ago inferred from molasse deposits along the Altyn Tagh fault. Earth Planet. Sci. Lett. 235, 641–653.
Suttner, L.J., Basu, A., 1985. The effect of grain size on detrital modes: a test of the Gazzi-Dickinson poing- counting method: discussion. J. Sediment. Petrol. 55, 616–617.
Tang, L.J., Jin, Z.J., Dai, J.S., Zhang, M.L., Zhang, B.S., 2002. Regional fault systems of Qaidam basin and adjacent orogenic belts. Earth Sci. 27, 666–682 (in Chinese with English abstract).
Tang, J., Zhan, Y., Zhao, G.Z., Deng, Q.H., Wang, J.J., Chen, X.B., Zhao, J.M., Xuan, F., 2005. Electrical conductivity structure of the crust and upper mantle in the northeastern margin of the Qinghai-Tibet plateau along the profile Maqên-Lanzhou-Jingbian. Chin. J. Geophys. 48, 1205–1216 (in Chinese with English abstract).
Tang, Z.H., Ding, Z.L., White, P.D., Dong, X.X., Ji, J.L., Jiang, H.C., Luo, P., Wang, X., 2011. Late Cenozoic central Asian drying inferred from a palynological record from the northern Tian Shan. Earth Planet. Sci. Lett. 302, 439–447.
Tian, J., Ma, W., Lyle, M.W., Shackford, J.K., 2014. Synchronous mid-Miocene upper and deep oceanic $\delta^{13}C$ changes in the east equatorial Pacific linked to ocean cooling and ice sheet expansion. Earth Planet. Sci. Lett. 406, 72–80.
Tu, D.L., Wang, Z.J., Zeng, B.H., Gao, Q., 1998. Study on distribution and activity characters of the Holocene faults in the Huangshui Basin, Qinghai Province. Northwest. Seismol. J. 20, 83–90 (in Chinese with English abstract).
Wan, J.L., Wang, Y., Li, Q., Wang, F., Wang, E.Q., 2001. FT evidence of northern Altyn uplift in late-Cenozoic. Bull. Mineral. Petrol. Geochem. 20, 222–224 (in Chinese with English abstract).
Wan, S.M., Li, A.C., Peter, D., Clift, J., Stuut, W., 2007. Development of the east Asian monsoon: mineralogical and sedimentologic records in the northern South China Sea since 20 Ma. Palaeogeogr. Palaeoclimatol. Palaeoecol. 152, 37–47.
Wang, J., Wang, Y.J., Liu, Z.C., Li, J.Q., Xi, P., 1999. Cenozoic environmental evolution of the Qaidam Basin and its implications for the uplift of the Tibetan plateau and the drying of Central Asia. Palaeogeogr. Palaeoclimatol. Palaeoecol. 152, 37–47.
Wang, G.H., Ran, S.M., Li, M., 2001. The characteristics of Neogene Serteng Shan-Xietie Shan oblique thrust fault in the northern margin of Qaidam Basin. J. Geom. 7, 224–230 (in Chinese with English abstract).
Wang, Y., Wan, J.L., Li, Q., Wang, F., Wang, E.Q., 2002. Fission-track evidence for the Cenozoic uplift and erosion of the northern segmeng of the Altyn Tagh fault zone at the Aksay-Dangjin pass. Acta Geol. Sin. 76, 191–198 (in Chinese with English abstract).
Wang, Y.D., Nie, J.S., Zhang, T., Sun, G.Q., Yang, X., Liu, Y.H., Liu, X.W., 2010. Cenozoic tectonic evolution in the western Qaidam Basin inferred from subsurface data. J. Geosci. 14, 335–344.
Wang, G.C., Cao, K., Zhang, K.X., Wang, A., Liu, C., Meng, Y.N., Xu, Y.D., 2011. Spatio-temporal framework of tectonic uplift stages of the Tibetan plateau in Cenozoic. Sci. China Ser. D Earth Sci. 54, 29–44.
Wang, J.Y., Fang, X.M., Appel, E., Song, C.H., 2012a. Pliocene-Pleistocene climate change at the NE Tibetan plateau deduced from lithofacies variation in the drill Core SG-1, western Qaidam Basin, China. J. Sediment. Res. 82, 933–952.
Wang, Z.C., Zhang, P.Z., Garzione, C.N., Lease, R.O., Zhang, G.L., Zheng, D.W., Hough, B., Yuan, D.Y., Li, C.Y., Liu, J.H., Wu, Q.L., 2012b. Magnetostratigraphy and depositional history of the Miocene Wushan basin on the NE Tibetan plateau, China: implications for middle Miocene tectonics of the west Qinling fault zone. J. Asian Earth Sci. 44, 189–202.
Wang, Y.D., Zheng, J.J., Zhang, W.L., Li, S.Y., Liu, X.W., Yang, X., Liu, Y.H., 2012c. Cenozoic uplift of the Tibetan plateau: evidence from the tectonic-sedimentary evolution of the western Qaidam Basin. Geosci. Front. 3, 175–187.
Wang, G.C., Zhang, K.X., Xiang, S.Y., Wang, A., Cao, K., 2014. Cenozoic Geological Map of the Qinghai- Tibetan Plateau and its Instruction. China University of Geosciences Press, Wuhan. pp. 1–153.
Wang, W.T., Zhang, P.Z., Liu, C.C., Zheng, D.W., Yu, J.X., Zheng, W.J., Wang, Y.Z., Zhang, H.P., Chen, X.Y., 2016a. Pulsed growth of the west Qinling at ~30 Ma in northeastern Tibet: evidence from Lanzhou Basin magnetostratigraphy and provenance. J. Geophys. Res. Solid Earth 121, 7754–7774.
Wang, W.T., Zhang, P.Z., Yu, J.X., Wang, Y.Z., Zheng, D.W., Zheng, W.J., Zhang, H.P., Pang, J.Z., 2016b. Constraints on mountain building in the northeastern Tibet: detrital zircon records from synorogenic deposits in the Yumen Basin. Sci. Rep. 6, 27604. http://dx.doi.org/10.1038/srep27604.
Wang, W.T., Zhang, P.Z., Zheng, W.J., Zheng, D.W., Liu, C.C., Xu, H.Y., Zhang, H.P., Yu, J.X., Pang, J.Z., 2016c. Uplift-driven sediment redness decrease at ~16.5 Ma in the Yumen Basin along the northeastern Tibetan plateau. Sci. Rep. 6, 29568. http://dx.doi.org/10.1038/srep29568.
Wang, W.T., Zheng, W.J., Zhang, P.Z., Li, Q., Kirby, E., Yuan, D.Y., Zheng, D.W., Liu, C.C., Wang, Z.C., Zhang, H.P., Pang, J.Z., 2017. Expansion of the Tibetan plateau during the Neogene. Nat. Commun. 8, 15887. http://dx.doi.org/10.1038/ncomms15887.
Wang, Y.Z., Zheng, D.W., Pang, J.Z., Zhang, H.P., Wang, W.T., Yu, J.X., Zhang, Z.Q., Zheng, W.J., Zhang, P.Z., Li, Y.J., 2018. Using slope-area and apatite fission track analysis to decipher the rock uplift pattern of the Yumu Shan: new insights into the growth of the NE Tibetan plateau. Geomorphology 308, 118–128.
Wu, L., Xiao, A.C., Yang, S.F., Wang, L.Q., Mao, L.G., Wang, L., Dong, Y.P., Xu, B., 2012. Two-stage evolution of the Altyn Tagh fault during the Cenozoic: new insight from provenance analysis of geological section in NW Qaidam Basin, NW China. Terra Nova 24, 387–395.
Xia, L.Q., Li, X.M., Ma, Z.P., Xu, X.Y., Xia, Z.C., 2011. Cenozoic volcanism and tectonic evolution of the Tibetan plateau. Gondwana Res. 19, 850–866.
Xiao, G.Q., Guo, Z.T., Dupont-Nivet, G., Lu, H.Y., Wu, N.Q., Ge, J.Y., Hao, Q.Z., Peng, S.Z., Li, F.J., Abels, H.A., Zhang, K.X., 2012. Evidence for northeastern Tibetan plateau uplift between 25 and 20 Ma in the sedimentary archive of the Xining Basin, northwestern China. Earth Planet. Sci. Lett. 317–318, 185–195.
Xu, Y.D., Zhang, K.X., Chen, R.M., Zhang, J.Y., 2013. Oligocene tectonic lithofacies paleogeography of the Tibetan plateau. Geol. Bull. China 32, 44–55 (in Chinese with English abstract).
Yan, M., Van Der, V.R., Fang, X.M., Pares, J.M., Rea, D.K., 2006. Paleomagnetic evidence for a mid- Miocene clockwise rotation of about 25° of the Guide Basin area in NE Tibet. Earth Planet. Sci. Lett. 241, 234–247.
Yan, X.L., Miao, Y.F., Zan, J.B., Zhang, W.L., Wu, S., 2014. Late Cenozoic fluvial-lacustrine susceptibility increases in the Linxia Basin and their implications for Tibetan plateau uplift. Quat. Int. 334–335, 132–140.
Yang, R.S., Fang, X.M., Meng, Q.Q., Zan, J.B., Zhang, W.L., Deng, T., Yang, Y.B., Ruan, X.B., Yang, L.Y., Li, B.S., 2017. Paleomagnetic constraints on the middle Miocene-early Pliocene stratigraphy in the Xining Basin, NE Tibetan plateau, and the geologic implications. Geochem. Geophys. Geosyst. 18, 3741–3757.
Yin, A., Dang, Y.Q., Wang, L.C., Jiang, W.M., Zhou, S.P., Chen, X.H., Gehrels, G.E., McRivette, M.W., 2008a. Cenozoic tectonic evolution of Qaidam basin and its surrounding regions (part 1): the southern Qilian Shan- Nan Shan thrust belt and northern Qaidam basin. Geol. Soc. Am. Bull. 120, 813–846.
Yin, A., Dang, Y.Q., Zhang, M., Chen, X.H., McRivette, M.W., 2008b. Cenozoic tectonic evolution of Qaidam basin and its surrounding regions (part 3): structural geology, sedimentation, and regional tectonic reconstruction. Geol. Soc. Am. Bull. 120, 847–876.
Yuan, D.Y., Liu, X.L., Liu, B.C., Zhang, P.Z., 2003a. A preliminary study on paleo-earthquake events of the Reishui-Riyue Mt., active fault zone in Qinghai Province. Northwest. Seismol. J. 25, 136–142 (in Chinese with English abstract).
Yuan, D.Y., Liu, B.C., Zhang, P.Z., Liu, B.C., 2003b. Characteristics of the modern activity of the Reshui-Riyueshan fault zone in Qinghai Province. Earthq. Res. China 25, 155–165 (in Chinese with English abstract).
Yuan, D.Y., Zhang, P.Z., Lei, D.S., Liu, B.C., Liu, X.L., 2005. A preliminary study on the new activity features of the Lajishan Mountain fault zone in Qinghai Province. Earthq. Res. China 21, 93–102 (in Chinese with English abstract).
Yuan, W.M., Dong, J.Q., Wang, S.C., Andrew, C., 2006. Apatite fission track evidence for Neogene uplift in the eastern Kunlun Mountains, northern Qinghai-Tibet plateau, China. J. Asian Earth Sci. 27, 847–856.
Zachos, J., Pagani, M., Sloan, L., Thomas, E., Billups, K., 2001. Trends, rhythms, and aberrations in global climate 65 Ma to present. Science 292, 686–693.
Zhang, X., Jiang, Z.S., Wang, Q., Wang, S.C., Cui, D.X., Zhang, X.L., 2004. Tectonic deformation features of the northern Tibetan plateau and their relationship to strong earthquakes. Prog. Geophys. 19, 363–371.
Zhang, Z.S., Wang, H.J., Guo, Z.T., Jiang, D.B., 2007. What triggers the transition of palaeoenvironmental patterns in China, the Tibetan plateau uplift or the Paratethys Sea retreat? Palaeogeogr. Palaeoclimatol. Palaeoecol. 245, 317–331.
Zhang, K.X., Wang, G.C., Cao, K., Liu, C., Zhu, Z.M., Xu, Y.D., Chen, F.N., Kou, X.H., Meng, Y.N., Chen, R.M., 2008. Cenozoic sedimentary records and geochronological constraints of differential uplift of the Qinghai-Tibet plateau. Sci. China Ser. D Earth Sci. 51, 1658–1672.
Zhang, K.X., Wang, G.C., Ji, J.L., Luo, M.S., Kou, X.H., Wang, Y.M., Xu, Y.D., Chen, F.N., Chen, R.M., Song, B.W., Zhang, J.Y., Liang, Y.P., 2010a. Paleogene- Neogene stratigraphic realm and sedimentary sequence of the Qinghai-Tibet plateau and their response to uplift of the plateau. Sci. China Ser. D Earth Sci. 84, 357–369.
Zhang, J.Y., Zhang, K.X., Ji, J.L., Luo, M.S., Chen, F.N., Xu, Y.D., Wang, Y.M., 2010b. Oligocene-Pliocene sedimentary facies analysis and sedimentary evolution of Xunhua Basin in northeastern margin of Qinghai-Tibet plateau. Earth Sci. 35, 774–788 (in Chinese with English abstract).
Zhang, C.F., Wang, Y., Li, Q., Wang, X.M., Deng, T., Tseng, Z.J., Takeuchi, G.T., Xie, G.P., Xu, Y.F., 2012. Diets and environments of late Cenozoic mammals in the Qaidam Basin, Tibetan plateau: evidence from stable isotopes. Earth Planet. Sci. Lett. 333-334, 70–82.
Zhang, W.L., Fang, X.M., Song, C.H., Erwin, A., Yan, M.D., Wang, Y.D., 2013. Late Neogene magnetostratigraphy in the western Qaidam Basin (NE Tibetan plateau) and its constraints on active tectonic uplift and progressive evolution of growth strata. Tectonophysics 599, 107–116.
Zhang, K.X., Wang, G.C., Luo, M.S., Ji, J.L., Xu, Y.D., Chen, R.M., Song, B.W., Chen, F.N., Liang, Y.P., Jiang, S.S., Cao, K., Wang, A., 2013a. Cenozoic Tectonic Lithofacies Paleogeography Map of the Qinghai- Tibetan Plateau and its Instruction. Geological

Publishing House, Beijing, pp. 1–299 (in Chinese with English abstract).
Zhang, K.X., Wang, G.C., Xu, Y.D., Luo, M.S., Ji, J.L., Xiao, G.Q., Wang, A., 2013b. Sedimentary evolution of the Qinghai- Tibetan plateau in Cenozoic and its response to the uplift of the plateau. Acta Geol. Sin. 76, 191–198 (in Chinese with English abstract).
Zhang, J., Wang, Y.N., Zhang, B.H., Zhang, Y.P., 2014. Tectonics of the Xining Basin in NW China and its implications for the evolution of the NE Qinghai-Tibetan plateau. Basin Res. 12104, 1–24. http://dx.doi.org/10.1111/bre.12104.
Zhang, J., Wang, Y.N., Zhang, B.H., Zhao, H., 2015a. Evolution of the NE Qinghai-Tibetan plateau, constrained by the apatite fission track ages of the mountain ranges around the Xining Basin in NW China. J. Asian Earth Sci. 97, 10–23.
Zhang, C.X., Xiao, G.Q., Guo, Z.T., Wu, H.B., Hao, Q.Z., 2015b. Evidence of late early Miocene aridification intensification in the Xining Basin caused by the northeastern Tibetan plateau uplift. Glob. Planet. Chang. 128, 31–46.
Zhang, T., Han, W.X., Fang, X.M., Zhang, W.L., Song, C.H., Yan, M.D., 2016. Intensified tectonic deformation and uplift of the Altyn Tagh range recorded by rock magnetism and growth strata studies of the western Qaidam Basin, NE Tibetan plateau. Glob. Planet. Chang. 137, 54–68.
Zhang, H.P., Zhang, P.Z., Prush, V., Zheng, D.W., Zheng, W.J., Wang, W.T., Liu, C.C., Ren, Z.K., 2017. Tectonic geomorphology of the Qilian Shan in the northeastern Tibetan plateau: insights into the plateau formation processes. Tectonophysics 706–707, 103–115.
Zheng, D.W., Zhang, P.Z., Wan, J.L., Li, C.Y., Cao, J.X., 2003. Late Cenozoic deformation subsequence in northeastern margin of Tibet-detrital AFT records from Linxia Basin. Sci. China Ser. D Earth Sci. 46, 266–275.
Zheng, D.W., Clark, M.K., Zhang, P.Z., Zheng, W.J., Kenneth, A.F., 2010. Erosion, fault initiation and topographic growth of the north Qilian Shan (northern Tibetan plateau). Geol. Soc. Am. Bull. 6, 937–941.
Zheng, D.W., Wang, W.T., Wan, J.L., Yuan, D.Y., Liu, C.R., Zheng, W.J., Zhang, H.P., Pang, J.Z., 2017. Progressive northward growth of the northern Qilian Shan-Hexi corridor (northeastern Tibet) during the Cenozoic. Lithosphere 9, 408–416.
Zhong, D.L., Ding, L., 1996. Raising process of the Qinghai-Xizang (Tibet) plateau and its mechanism. Sci. China Ser. D Earth Sci. 39, 369–379.
Zhou, H., Chen, L., Diwu, C.R., Lei, C., 2018. Cenozoic uplift of the Qimantage Mountains, northeastern Tibet: Contraints from provenance analysis of Cenozoic sediments in Qaidam Basin. Geol. J. 1–20. http://dx.doi.org/10.1002/gj.3095.
Zhu, L.D., Wang, C.S., Zheng, H.B., Xiang, F., Yi, H.S., Liu, D.Z., 2006. Tectonic and sedimentary evolution of basins in the northern of Qinghai-Tibet plateau and their implication for the northward growth of the plateau. Palaeogeogr. Palaeoclimatol. Palaeoecol. 241, 49–60.
Zhuang, G.S., Hourigan, J.K., Koch, P.L., Ritts, B.D., Kent-Corson, M.L., 2011. Isotopic constraints on intensified aridity in Central Asia around 12 Ma. Earth Planet. Sci. Lett. 312, 152–163.
Zhuang, G.S., Johnstone, S., Hourigan, J., Lippert, P., Ritts, B., Robinson, A., Sobel, E.R., 2018. Understanding the geologic evolution of Northern Tibetan Plateau with multiple thermochronometers. Gondwana Res. http://dx.doi.org/10.1016/j.gr.2018.02.014. in press.